

FORMULATION OF SILYMARIN NANOEMULSIONS FOR DERMAL DELIVERY

Miss Ranit Charoenjittichai



บทคัดย่อและแฟ้มข้อมูลฉบับเต็มของวิทยานิพนธ์ตั้งแต่ปีการศึกษา 2554 ที่ให้บริการในคลังปัญญาจุฬาฯ (CUIR)
เป็นแฟ้มข้อมูลของนิสิตเจ้าของวิทยานิพนธ์ ที่ส่งผ่านทางบัณฑิตวิทยาลัย

The abstract and full text of theses from the academic year 2011 in Chulalongkorn University Intellectual Repository (CUIR)
are the thesis authors' files submitted through the University Graduate School.

A Thesis Submitted in Partial Fulfillment of the Requirements
for the Degree of Master of Science Program in Pharmaceutical Technology

Department of Pharmaceutics and Industrial Pharmacy

Faculty of Pharmaceutical Sciences

Chulalongkorn University

Academic Year 2016

Copyright of Chulalongkorn University

การตั้งตำรับซีลีมารินนาโนอิมัลชันสำหรับการนำส่งเข้าผิวหนัง



วิทยานิพนธ์นี้เป็นส่วนหนึ่งของการศึกษาตามหลักสูตรปริญญาวิทยาศาสตรมหาบัณฑิต
สาขาวิชาเทคโนโลยีเภสัชกรรม ภาควิชาวิทยาการเภสัชกรรมและเภสัชอุตสาหกรรม

คณะเภสัชศาสตร์ จุฬาลงกรณ์มหาวิทยาลัย

ปีการศึกษา 2559

ลิขสิทธิ์ของจุฬาลงกรณ์มหาวิทยาลัย

Thesis Title	FORMULATION OF SILYMARIN NANOEMULSIONS FOR DERMAL DELIVERY
By	Miss Ranit Charoenjittichai
Field of Study	Pharmaceutical Technology
Thesis Advisor	Assistant Professor Vipaporn Panapisal, Ph.D.
Thesis Co-Advisor	Dusadee Charnvanich, Ph.D.

Accepted by the Faculty of Pharmaceutical Sciences, Chulalongkorn
University in Partial Fulfillment of the Requirements for the Master's Degree

.....Dean of the Faculty of Pharmaceutical Sciences
(Assistant Professor Rungpetch Sakulbumrungsil, Ph.D.)

THESIS COMMITTEE

.....Chairman
(Assistant Professor Nontima Vardhanabhuti, Ph.D.)

.....Thesis Advisor
(Assistant Professor Vipaporn Panapisal, Ph.D.)

.....Thesis Co-Advisor
(Dusadee Charnvanich, Ph.D.)

.....Examiner
(Associate Professor Warangkana Warisnoicharoen, Ph.D.)

.....External Examiner
(Veerawat Teeranachaideekul, Ph.D.)

รณิศ เจริญจิตติชัย : การตั้งตำรับซิลิมารินนาโนอิมัลชันสำหรับการนำส่งเข้าผิวหนัง (FORMULATION OF SILYMARIN NANOEMULSIONS FOR DERMAL DELIVERY) อ.ที่ปรึกษาวิทยานิพนธ์หลัก: ผศ. ภาณุ. ดร.วิภาพร พนาพิศาล, อ.ที่ปรึกษาวิทยานิพนธ์ร่วม: อ. ภาณุ. ดร.ศุภฎี ขาญวานิช, 96 หน้า.

ซิลิมารินเป็นสารสกัดมาตรฐานจากเมล็ดของ *Silybum marianum* ซึ่งนิยมใช้สำหรับรักษาโรคเกี่ยวกับตับ จากรายงานการศึกษาคุณสมบัติของซิลิมาริน พบว่าซิลิมารินมีประโยชน์สามารถใช้ในผิวหนัง ได้แก่ ฤทธิ์ต้านอนุมูลอิสระ ฤทธิ์ต้านเอนไซม์ไทโรซิเนส ฤทธิ์ต้านการอักเสบ รวมถึงฤทธิ์ต้านมะเร็ง เป็นต้น การนำส่งซิลิมารินเข้าสู่ผิวหนังจึงมีความน่าสนใจและมีความท้าทาย การศึกษานี้มีวัตถุประสงค์เพื่อพัฒนาตำรับซิลิมารินนาโนอิมัลชันที่เหมาะสมสำหรับนำส่งเข้าผิวหนัง นาโนอิมัลชันชนิดอิมัลชันน้ำในน้ำเตรียมโดยใช้วิธี High-pressure homogenization โดยมี Caprylic/capric triglycerides เป็นตัวทำละลายในน้ำ สารลดแรงตึงผิวผสมระหว่าง Tween[®] 20 และ Transcutol[®] ซึ่งผสมในอัตราส่วนต่างกัน และความเข้มข้นต่างกัน นาโนอิมัลชันที่เตรียมได้จะถูกประเมินลักษณะทางกายภาพ ขนาดอนุภาค การกระจายของขนาดอนุภาค นอกจากนี้ยังประเมินความคงตัวของกายภาพด้วยวิธีการปั่นเหวี่ยง การเก็บที่อุณหภูมิร้อนสลับเย็น และ อัตราการเกิดออกสเตอไรต์ไร้เพนนิ่งที่อุณหภูมิห้อง ผลปรากฏว่า ขนาดอนุภาคของนาโนอิมัลชันเปล่า อยู่ในช่วงระหว่าง 88.3 ถึง 227.2 นาโนเมตร ซึ่งมีการกระจายของขนาดอนุภาค อยู่ในช่วงระหว่าง 0.086 ถึง 0.197 การเพิ่มความเข้มข้นของสารลดแรงตึงผิวผสมทำให้ขนาดอนุภาคเล็กลง อย่างไรก็ตาม จากการศึกษาพบว่าสูตรตำรับที่มีปริมาณ Tween[®] 20, Transcutol[®] หรือปริมาณสารลดแรงตึงผิวผสมที่มากจะส่งผลให้อัตราการเกิดออกสเตอไรต์ไร้เพนนิ่งมากตามไปด้วย ซึ่งส่งผลให้ตำรับนาโนอิมัลชันสูตรนั้นไม่คงตัว เมื่อเก็บไว้ที่สภาวะเร่งอุณหภูมิร้อนสลับเย็น สูตรตำรับนาโนอิมัลชันที่มีเฉพาะ Tween[®] 20 (สูตร F1) มีอัตราการเกิดออกสเตอไรต์ไร้เพนนิ่งต่ำที่สุดที่ 368.24 ลูกบาศก์นาโนเมตรต่อชั่วโมง และเลือกสูตรตำรับนี้สำหรับพัฒนาความคงตัวในสภาวะเร่งอุณหภูมิร้อนสลับเย็น โดยเพิ่มสารก่อเจล Carbopol[®] 940 (0.2 %w/w) จากนั้นพัฒนาต่อด้วยการเติมสารสกัดซิลิมารินจำนวน 0.5 %w/w ซึ่งเป็นปริมาณความเข้มข้นมากที่สุดที่สามารถเข้ากับนาโนอิมัลชันเจลสูตรนี้ได้ ขนาดอนุภาคของซิลิมารินนาโนอิมัลชันเจล คือ 112.7 นาโนเมตร และมีค่าการกระจายของขนาดอนุภาคที่ 0.208 ผลการศึกษาความคงตัวของสูตรตำรับซิลิมารินนาโนอิมัลชันเจล พบว่า คงตัวได้ดีและผ่านการทดสอบในสภาวะเร่งอุณหภูมิร้อนสลับเย็นครบจำนวน 6 รอบ ผลการศึกษาปริมาณสารสำคัญซิลิมารินในสูตรตำรับนี้ พบ 0.527 %w/w ซึ่งมีการสลายตัวระหว่างการเก็บซิลิมารินนาโนอิมัลชันเจลที่อุณหภูมิ 40 องศาเซลเซียส เป็นเวลา 3 เดือน นอกจากนี้ความสามารถในการกักเก็บซิลิมารินของสูตรนาโนอิมัลชันนี้ คือ 83.91 % ปริมาณสะสมจากการปลดปล่อยซิลิมารินจากตำรับซิลิมารินนาโนอิมัลชันเจลมากกว่าการปลดปล่อยซิลิมารินจากตำรับซิลิมารินไมโครอิมัลชัน ซึ่งผลการทดลองสอดคล้องกับสมมติฐานที่ว่า ความชอบของยาต่อระบบมีน้อยกว่าในตำรับนาโนอิมัลชัน เพราะมีปริมาณสารลดแรงตึงผิวน้อยกว่า ซึ่งส่งผลให้ปลดปล่อยซิลิมารินออกมาได้มากกว่า การศึกษาต่อไปควรศึกษาการซึมผ่านผิวหนังของสูตรตำรับซิลิมารินนาโนอิมัลชันเทียบกับตำรับซิลิมารินไมโครอิมัลชัน รวมถึงความระคายเคืองต่อผิว และประสิทธิภาพในการออกฤทธิ์อื่นๆ ต่อผิวหนัง

ภาควิชา วิทยาการเภสัชกรรมและเภสัชอุตสาหกรรม ลายมือชื่อนิสิต

สาขาวิชา เทคโนโลยีเภสัชกรรม ลายมือชื่อ อ.ที่ปรึกษาหลัก

ปีการศึกษา 2559 ลายมือชื่อ อ.ที่ปรึกษาร่วม

5676358233 : MAJOR PHARMACEUTICAL TECHNOLOGY

KEYWORDS: SILYMARIN / NANOEMULSIONS / SKIN DELIVERY

RANIT CHAROENJITTICHA: FORMULATION OF SILYMARIN NANOEMULSIONS FOR DERMAL DELIVERY. ADVISOR: ASST. PROF. VIPAPORN PANAPISAL, Ph.D., CO-ADVISOR: DUSADEE CHARNVANICH, Ph.D., 96 pp.

Silymarin, a standardized extract from the seeds of *Silybum marianum*, has been used for liver diseases and recently it was reported to have many skin benefits including antioxidant, anti-tyrosinase, anti-inflammatory and antitumor. Delivery of silymarin through the skin has been an attractive as well as a challenging area for research. The present study aims to develop an optimal nanoemulsion containing silymarin using different surfactant mixture (smix) ratios and concentrations. Oil-in-water nanoemulsions were prepared by high-pressure homogenization method. Caprylic/capric triglycerides was used as an oil phase. Surfactant mixtures between Tween[®] 20 and Transcutol[®] were varied with different ratios and concentrations. Nanoemulsions were characterized for physical appearances, particle size and size distribution. Their physical stabilities were tested using centrifugation, heating-cooling cycle, and Ostwald ripening rate after storage at room temperature. The mean particle sizes of blank nanoemulsions were in the range of 88.3 to 227.2 nm with polydispersity index of 0.086 to 0.197. An increase in smix concentration resulted in smaller particle size. However, high Tween[®] 20, Transcutol[®], or total smix concentration showed high Ostwald ripening rate and resulted in unstable nanoemulsions when stored in accelerated conditions. Nanoemulsion containing only Tween[®] 20 (F1 formulation) presented the lowest Ostwald ripening rate of 368.24 nm³/h and was selected. Carbopol[®] 940 (0.2 %w/w) was used as a gelling agent to improve the stability of nanoemulsion in heating-cooling cycles. 0.5 %w/w of silymarin was the maximum concentration that could be incorporated into nanoemulsion gel (SMNE gel). The particle size of SMNE gel was 112.7 nm with polydispersity index of 0.208. It showed good physical stability and passed six cycles of heating-cooling study. Consequently, silymarin content was 0.527 %w/w and gradually degraded during storage at 40 °C for three months. The entrapment efficiency of SMNE gel was 83.91 %. SMNE gel showed higher *in vitro* release of silymarin than silymarin microemulsion. The results supported our hypothesis that lower drug-system affinity in nanoemulsion which due to less surfactant should result in higher amount of silymarin released. For further studies, skin permeation of SMNE gel should be performed to compare with silymarin microemulsion, as well as skin irritation and its efficacy.

Department: Pharmaceutics and Industrial
 Pharmacy

Field of Study: Pharmaceutical Technology

Academic Year: 2016

Student's Signature

Advisor's Signature

Co-Advisor's Signature

ACKNOWLEDGEMENTS

This thesis would not be successful without the great supports from a number of people who have made their kind contributions to the study.

First of all, I would like to express my profound gratitude to my thesis advisor, Assistant Professor Dr. Vipaporn Panapisal, for her excellent advice, valuable encouragement and understanding throughout my research study.

I would like to express my sincere appreciation to Dr. Dusadee Charnvanich, my thesis co-advisor, for her warm support and kind suggestion.

I am also deeply thankful to Assistant Professor Dr. Nontima Vardhanabhuti, chairman of my thesis examination committee, as well as committee members, Associate Professor Dr. Warangkana Warisnoicharoen and Dr. Veerawat Teeranachaideekul for their valuable comments and helpful discussion.

I am appreciated to thank Berlin Pharmaceutical Co., Ltd. for supporting silymarin extract.

I am very thankful to all staff members of Department of Pharmaceutics and Industrial Pharmacy and staff members of Pharmaceutical Research Instrument Center for facilitating instruments and recommendation of uses. Thanks are also extended to staff of Pharmaceutical Technology Program.

I am very grateful to all my friends of Pharmaceutical Technology program, Cosmetic Science program, and Pharmaceutics program for their friendships, kind helps and gorgeous discussion.

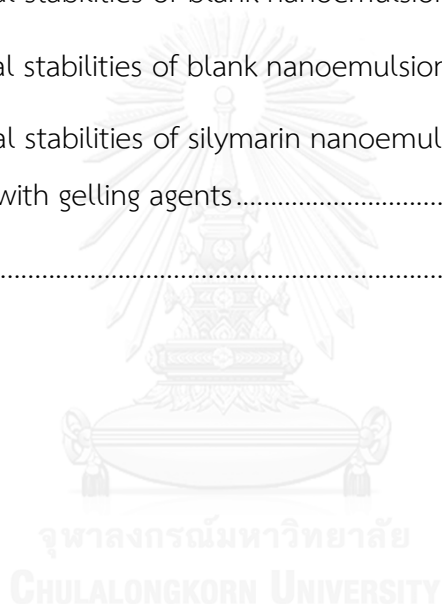
My deep gratitude is dedicated to my family for their endless love, understanding and encouragement.

CONTENTS

	Page
THAI ABSTRACT	iv
ENGLISH ABSTRACT	v
ACKNOWLEDGEMENTS	vi
CONTENTS	vii
LIST OF TABLES	x
LIST OF FIGURES	xi
LIST OF EQUATIONS	xiii
LIST OF ABBREVIATIONS	xiv
CHAPTER 1 INTRODUCTION	1
CHAPTER 2 LITERATURE REVIEW	5
1. Silymarin	5
2. Skin benefits of silymarin	7
3. Skin delivery of silymarin	8
4. Nanoemulsion development for skin delivery	10
CHAPTER 3 MATERIALS AND METHODS	13
Chemicals	13
Apparatus	14
Materials	15
Methods	16
A. Development and characterization of blank nanoemulsions	16
1. Preparation of blank nanoemulsions	16
2. Effects of smix ratio and smix concentration on physical properties and stabilities of blank nanoemulsions	16

	Page
3. Stabilization of nanoemulsions using gelling agent.....	17
B. Preparation of silymarin nanoemulsion	18
C. Characterization of blank and silymarin nanoemulsions	18
1. Physical properties	18
2. Physical stabilities.....	20
3. Chemical stability	21
4. <i>In vitro</i> release study.....	21
D. Quantitative analysis of silymarin by high performance liquid chromatographic (HPLC) method.....	23
E. Quantitative analysis of silymarin by UV-Vis spectrophotometric method ...	27
F. Statistical analysis	29
CHAPTER 4 RESULTS AND DISCUSSION.....	30
A. Development and characterization of blank nanoemulsions	30
1. Development of blank nanoemulsions.....	30
2. Effects of smix ratio and smix concentration on physical properties and stabilities of blank nanoemulsions	33
3. Stabilization of nanoemulsions using gelling agent.....	35
B. Preparation of silymarin nanoemulsion.....	39
C. Characterization of silymarin nanoemulsion gel	45
1. Entrapment efficiency (EE).....	45
2. Drug content	46
3. Chemical stability	46
4. <i>In vitro</i> release study	48

	Page
D. Quantitative analysis of silymarin by high performance liquid chromatographic (HPLC) method	50
E. Quantitative analysis of silymarin by UV-Vis spectrophotometric method.....	57
CHAPTER 5 CONCLUSIONS.....	61
REFERENCES	62
APPENDICES.....	69
APPENDIX A Physical stabilities of blank nanoemulsions.....	70
APPENDIX B Physical stabilities of blank nanoemulsions with gelling agents	78
APPENDIX C Physical stabilities of silymarin nanoemulsions and silymarin nanoemulsion with gelling agents.....	88
VITA.....	96



LIST OF TABLES

	PAGE
Table 1 Composition of blank nanoemulsions	17
Table 2 Physical properties and stabilities of blank nanoemulsions	31
Table 3 Size and size distribution of blank nanoemulsions with gelling agents	36
Table 4 pH and viscosity of blank nanoemulsions with gelling agents	37
Table 5 Physical properties and stabilities of blank nanoemulsions with gelling agents	38
Table 6 Physical properties and physical stabilities of silymarin nanoemulsions.....	40
Table 7 Physical properties and physical stabilities of silymarin nanoemulsions (F1) with 0.2 %w/w Carbopol [®] 940	44
Table 8 The data of silybin for calibration curve by HPLC method.....	53
Table 9 The data of silymarin for calibration curve by HPLC method	54
Table 10 The percentages of analytical recovery of silymarin by HPLC method.....	55
Table 11 Data of repeatability of silymarin by HPLC method.....	56
Table 12 Data of intermediate precision of silymarin by HPLC method	56
Table 13 The calibration curve data of silymarin in methanolic solution by UV-Vis spectrophotometric method	58
Table 14 The percentage of analytical recovery of silymarin in methanolic solution by UV-Vis spectrophotometric method	59
Table 15 Data of repeatability of silymarin by UV-Vis spectrophotometric method..	60
Table 16 Data of intermediate precision of silymarin by UV-Vis spectrophotometric method	60

LIST OF FIGURES

	PAGE
Figure 1 Structures of silybin A and silybin B.....	5
Figure 2 Other flavonolignans found in silymarin	6
Figure 3 Physical appearances of (a) freshly prepared blank nanoemulsion F1 and (b) freshly prepared blank nanoemulsions F1, F5, F10 and F11 from left to right, respectively.....	30
Figure 4 Physical appearances of blank nanoemulsions after centrifugation	32
Figure 5 Physical appearances of 0.5 %, 0.75 %, 1 %, 1.5 %w/w silymarin nanoemulsions (F1) after centrifugation from left to right, respectively.....	39
Figure 6 Physical appearances of (a) freshly prepared 0.5 %, 0.75 % and 1 %w/w silymarin nanoemulsions (F1) from left to right respectively. (b) Physical appearances of 0.5 %, 0.75 % and 1 %w/w silymarin nanoemulsions (F1) after one cycle of heating-cooling cycles.....	40
Figure 7 Physical appearances of 0.5 %, 0.75 %, 1 %w/w silymarin nanoemulsions (F5) after centrifugation from left to right, respectively	42
Figure 8 (a) Physical appearances of freshly prepared 0.5 %w/w (left) and 0.75 %w/w (right) silymarin nanoemulsions (F1) with 0.2 %w/w Carbopol [®] 940. (b) Physical appearances of 0.5 %w/w (left) and 0.75 %w/w (right) silymarin nanoemulsions (F1) with 0.2 %w/w Carbopol [®] 940 after stored for six cycles of heating-cooling cycles.	43
Figure 9 Silymarin nanoemulsion gels after ultracentrifugation at (a) 40,000 rpm, (b) 50,000 rpm, (c) 60,000 rpm and (d) 65,000 rpm for one hour at 25 °C.....	45
Figure 10 Chemical stabilities of silymarin nanoemulsion gel at 40 °C.	47
Figure 11 Release profiles of silymarin nanoemulsion gel (SMNE gel), silymarin microemulsion (SMME) and silymarin solution (mean ± SD, n=3).....	49

Figure 12 HPLC Chromatograms of (a) silymarin nanoemulsion gel, (b) blank nanoemulsion gel, (c) silymarin methanolic solution, (d) silybin and (e) methanol.... 51

Figure 13 Calibration curve of silybin by HPLC method..... 53

Figure 14 Calibration curve of silymarin by HPLC method..... 54

Figure 15 Calibration curve of silymarin in methanolic solution by UV-Vis spectrophotometric method 59



LIST OF EQUATIONS

	PAGE
Equation 1 Percentage Entrapment efficiency	19
Equation 2 Ostwald ripening rate	20
Equation 3 Limit of detection	25
Equation 4 Limit of quantitation.....	26
Equation 5 Stokes' Law	32



LIST OF ABBREVIATIONS

ANOVA	analysis of variance
g	gram
mg	milligram
mL	milliliter
N/A	not available
nm	nanometer
pH	potential hydrogen
rpm	revolutions per minute
SD	standard deviation
UV	ultraviolet
UV-Vis	ultraviolet to visible
w/w	weight by weight
µg	microgram
µL	microliter
°C	degree Celcius
%	percentage

CHAPTER 1

INTRODUCTION

Background of study

Silymarin, a mixture of flavonolignans, is obtained from the seed of milk thistle (*Silybum marianum* L. Gaertner). It is typically used for liver disease treatment and recently it showed some skin benefits such as anti-inflammatory, anti-tumor, anti-tyrosinase, UVA and UVB protection, and fibroblast proliferation (Ashkani-Esfahani et al., 2013; Choo et al., 2009; Han et al., 2007; Katiyar et al., 1997; Svobodova et al., 2007). Topical application of silymarin cream (7 and 14 mg/mL) effectively treated skin pigments in melasma patients and the percentage of lesion size significantly reduced from the first week of treatment (Altaei, 2012). Moreover, there were no side effects found in female melasma patients treated with silymarin cream (14 mg/mL) for three months (Elfar and El-Maghraby, 2015). In addition, w/o emulsion containing 4 % milk thistle seed extract presented anti-inflammatory effect by reducing skin erythema, anti-aging property, and also improving skin condition and skin appearance (Rasul et al., 2011; Rasul and Akhtar, 2012). Oil in water emulsion containing 10 % w/w silymarin showed the Sun Protection Factor (SPF) of 9 which was comparable to octyl methoxycinnamate (SPF 10.42), known as a UV filter (Couteau et al., 2007; 2011). Furthermore, silymarin nanoliposome presented higher killing rate of isolated methicillin-resistant *Staphylococcus aureus* (MRSA) strain when was compared with free silymarin (Faezizadeh, Gharib and Godarzee, 2015).

Large molecules of flavonolignan group limited solubility of silymarin in water and caused poor permeability through biological membranes (Theodosiou et al., 2014). In previous report of Woo et al. (2007), silymarin showed very low soluble in water (0.4 mg/mL); therefore, self-microemulsifying drug delivery system was used to

improve its solubility and oral bioavailability. Another system contained high amount of surfactant, microemulsion, can also improve silymarin's solubility. In contrast, drug may have strong affinity with the system and will not release from the system. The study of Panapisal team (2012) reported that *in vitro* skin permeation study of 2 % w/w silymarin microemulsions showed no silybin content in the receptor solution, but found in the donor compartment and skin extract. Authors explained that silymarin would rather be in the system than get into the skin because of high amount of surfactant and co-surfactant used. In correspondence, o/w emulsions containing silymarin-cyclodextrin complex showed no epidermis penetration of silymarin or no presence of silymarin in the receptor medium which may be caused by the same reason (Spada et al., 2013).

Less amount of surfactant and co-surfactant presented in nanoemulsion when compared with microemulsion may lower drug-system affinity. Moreover, it could reduce skin irritation and still maintain solubilized capacity of poorly soluble drug (Rocha-Filho et al., 2014). Various poorly soluble drugs have been employed in nanoemulsion formulations which has gained more attention for skin delivery due to its high entrapment efficiency, prolonged release, and skin permeation enhancement (Clares et al., 2014; Junyaprasert et al., 2009; Teeranachaideekul et al., 2007). Therefore, nanoemulsion is chosen as delivery system in this study.

Nanoemulsion is optically translucent to opaque flowable liquid due to its droplet size ranging between 20-200 nm (Gutiérrez et al., 2008). It is kinetically stable and non-equilibrium system. Energy is required in nanoemulsion formation because it could not form spontaneously. The production of nanoemulsion can be both low-energy (e.g. phase inversion temperature method and spontaneous emulsification) and high-energy (e.g. ultrasonication and high-pressure homogenization (HPH)) methods. A comparative study of nanoemulsion preparation methods was reported that nanoemulsion prepared using HPH method produced better characteristics than

that of nanoemulsion prepared using spontaneous emulsification in terms of particle size and size distribution (Sharma et al., 2015). The HPH production parameters including pressure, number of cycles, and temperature were reported to have an effect on particle size of nanoemulsions (Sharma et al., 2015; Wang et al., 2008; Yuan et al., 2008). Therefore, HPH method was used in this study and those production parameters were standardized.

In general, nanoemulsion consists of three main compositions namely oil, surfactant (and co-surfactant), and water. Surfactant and co-surfactant are considered as important parts which can influence nanoemulsion formation by lowering the interfacial tension. Surfactants also prevented coalescence of a new droplet formation which may affect nanoemulsion stability (Tadros et al., 2004). The surfactant type and concentration were varied in β -carotene nanoemulsion formulations which the study showed both surfactant type and concentration had effects on particle size and size distribution (Yuan et al., 2008). Normally, co-surfactant is typically short to medium chain alcohol which locates between the hydrophobic chain of surfactant to stabilize interfacial layer of nanoemulsion. Hence, the concentration and the ratio of surfactant and co-surfactant mixture (smix) are important factors for the small droplet formation and the system stability. Therefore, the smix concentration and smix ratio were studied. The group of Panapisal (2012) reported that silymarin microemulsions showed more chemically stable than silymarin solution and they expected that drug may locate between surfactant interfaces because of its high solubility in surfactant/co-surfactant. Therefore, the selection of surfactant and co-surfactant is considered important. According to previous report (Woo et al., 2007), silymarin showed very high soluble in diethylene glycol monoethyl ether (Transcutol[®]; 350.1 mg/mL). Transcutol[®] is considered safe with low toxicity (Sullivan Jr, Gad and Julien, 2014), which is suitable for pharmaceutical uses, especially topical application. Transcutol[®] was selected as a

co-surfactant in this study to improve silymarin loading as well as its stability. Compositions of nanoemulsions containing Transcutol[®] with non-ionic surfactants are obtained from literatures (Alvarado et al., 2015; Dixit, Kohli and Baboota, 2008; Kumar et al., 2009; Tang, Shridharan and Sivakumar, 2013).

Therefore, aims of this study are to develop silymarin nanoemulsions and to study effects of surfactant : co-surfactant ratio and concentration on appearances, particle size and size distribution, physical and chemical stabilities of silymarin nanoemulsions. In addition, *in vitro* releases of nanoemulsion and microemulsion (GL11, Panapisal et al. (2012)) were compared to proof our hypothesis. Silymarin microemulsion GL11 was chosen because it revealed the highest drug content in the skin extract.

Objectives of study

1. To study influence of nanoemulsion compositions on physical properties and stabilities of blank nanoemulsions
2. To evaluate physical and chemical properties of silymarin loaded nanoemulsions
3. To compare *in vitro* drug releases between silymarin nanoemulsion and microemulsion

CHAPTER 2

LITERATURE REVIEW

1. Silymarin

Silymarin is a mixture of flavonolignans, which are obtained from the seed of milk thistle (*Silybum marianum* L. Gaertner). Silymarin contains approximately 70 – 80 % flavonolignans namely silybin (silibinin), isosilybin, silychristin, silydianin and 2,3-dehydrosilybin and 20 – 30 % of polymeric or oxidized polyphenolic compounds (Křen and Walterová, 2005). The major compounds of silymarin complex are silybin A and silybin B (Figure 1), which are diastereomers with ratio nearly 1:1. The other compounds found in silymarin are shown in Figure 2. By considering their structures with polyphenol groups, which commonly are groups of flavonoid, showed very strong antioxidant and pharmacological activities.

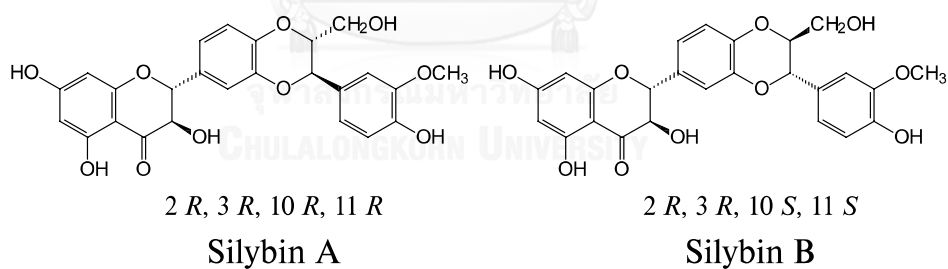


Figure 1 Structures of silybin A and silybin B
(Křen and Walterová, 2005)

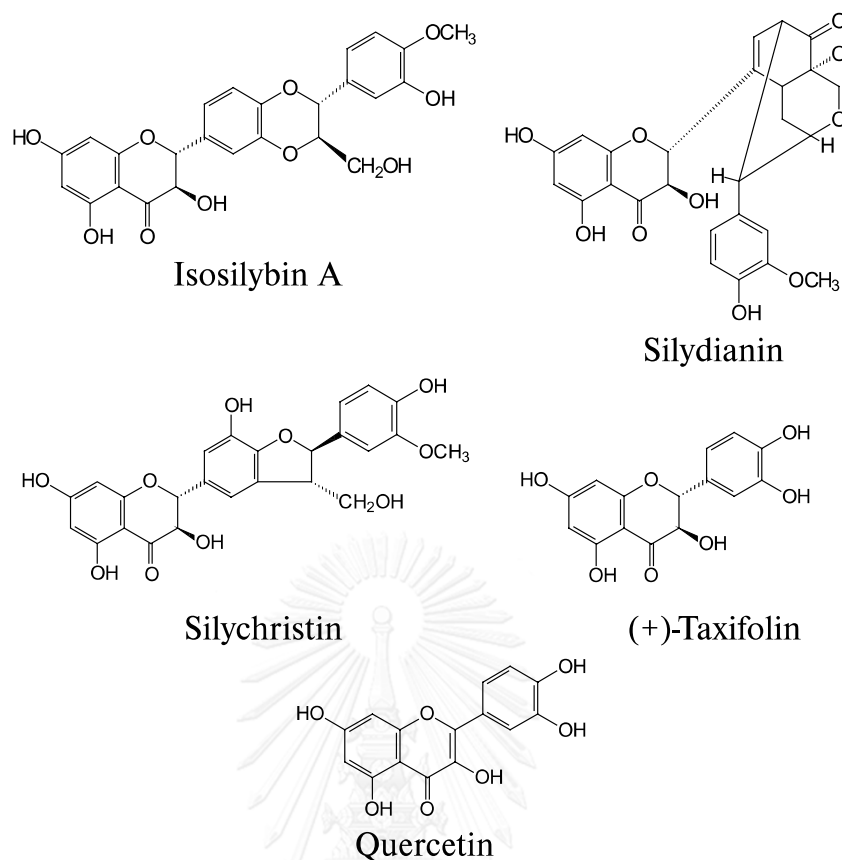


Figure 2 Other flavonolignans found in silymarin

(Křen and Walterová, 2005)

Antioxidant properties of silymarin were studied (Koksal et al., 2009). The results showed that lipid peroxidation inhibition of silymarin (82.7 %) was comparatively effective with BHA (83.3 %), BHT (82.1 %) and trolox (81.3 %) at the same concentration of 30 $\mu\text{g/mL}$. Moreover, the results of silymarin on free radical scavenging activity showed EC_{50} of 20.8 $\mu\text{g/mL}$ (DPPH assay) and EC_{50} of 8.62 $\mu\text{g/mL}$ (ABTS assay). More precisely, seven major components of silymarin were studied on free radical scavenging, which taxifolin showed the most effective in DPPH assay with EC_{50} of 32 μM (Anthony and Saleh, 2013). Although, taxifolin, non-flavonolignan, was only 3.5 % found in silymarin but it showed more potent than silybin A and silybin B, major components in silymarin with EC_{50} of 311 and 344 μM , respectively. Those results was consistency with the previous studies of Gazak et al. (2004) that taxifolin

(IC₅₀ of 21 μ M) was stronger activity than that of silybin (IC₅₀ of 1745 μ M) in DPPH assay. In addition, silymarin and its components were considered as safe with no cytotoxicity because it has been used to treat liver disease for a long time.

2. Skin benefits of silymarin

Skin is an outermost part of body and has very large area confronted with harmful environment e.g. UV radiation, chemicals, and animals, causing skin diseases. Both UVA and UVB induce the generation of ROS in skin cells, which are related to any stages of skin aging and skin carcinogenesis. As the structures of silymarin are polyphenols, they possess the abilities to be a skin photo-protection. There are the studies of photo-protective potencies of silymarin done by Katiyar teams. The application of silymarin to female SKH-1 hairless mice induced by UVB radiation showed less sunburn, apoptotic cells and skin edema formation (Katiyar et al., 1997). It also decreased catalase activity, induction of cyclooxygenase and ornithine decarboxylase (ODC) activities, and ODC mRNA expression in short-term study. For long-term studies, silymarin could reduce tumor incidence in all different stages of photo-carcinogenesis (initiation, promotion and complete carcinogenesis). Moreover, the JB6 C141 cells (preneoplastic epidermal keratinocytes) and p53^{+/+} fibroblasts were treated with silymarin and silibinin, showed that silymarin-induced apoptosis was primarily p53 dependent and mediated through the activation of caspase-3 (Katiyar, Roy and Baliga, 2005). Silymarin could also protect C3H/HeN mice from UVB-induced immunosuppression and showed inhibition of interleukin (IL)-10 and induction of IL-12 (Meeran et al., 2006). Moreover, pre-treatment with silymarin and its compounds on human keratinocyte (HaCaT) and mouse fibroblast (BALB/c) induced oxidative stress by hydrogen peroxide could reduce oxidative injury (Svobodova, Walterova and Psotova, 2006). Cytoprotection of silymarin on both

HacaT and BALB/c was comparable to silybin, while dehydrosilybin and quercetin revealed the most powerful protectants when analyzed by neutral red retention and lactate dehydrogenase (LDH) leakage. The results correlated to their potencies on antioxidant activities. Consequently, silymarin was suggested to be used for detoxifying ROS skin inflammation and preventing skin oxidative damage, which could regenerate new skin in case of wound healing (Svobodova et al., 2006). These promising results showed that silymarin was very effective for skin protection and proliferation.

After that, 2 % silymarin gel was applied on Wistar rats with 1 cm² full-thickness wound (Ashkani-Esfahani et al., 2013). The results showed that silymarin gel significant increased number density of fibroblast proliferation, % volume density of collagen bundle synthesis and volume density of hair follicle. On the other hand, angiogenesis was not significantly different from control and gel-base group.

Moreover, silymarin could be used as a natural skin lightening agent as it showed depigmentation effect in mouse melanocyte cell line (Mel-Ab) by decreasing tyrosinase protein expression and leading to melanogenesis inhibition (Choo et al., 2009). After that, the clinical studies on melasma patients with 7 and 14 mg/mL of silymarin cream (Altaei, 2012) and 14 mg/mL (Elfar and El-Maghraby, 2015) effectively treated skin pigment and showed no side effects.

3. Skin delivery of silymarin

Most compounds are possible permeated the skin through combination pathways which are intercellular route, transcellular route and appendage. Physicochemical properties of compounds influence to skin permeation. For example, molecular size should be less than 500 Da, where molecular size of

silymarin is 482.1 Da (Davis-Searles et al., 2005). An optimal partition coefficient ($\log P_{o/w}$) of permeant is about 2-3, which is related to lipophilic environment for intercellular diffusion. $\log P_{o/w}$ of silymarin is 2.7 (Woo et al., 2007). Limited water solubility of silymarin leads some difficulties in topical formulation development. Those physicochemical properties of silymarin are attractive and challenging to deliver on the skin, into the skin or even into blood circulation in order to avoid first pass metabolism.

Topical delivery of silymarin constituents including silybin, silydianin and silychristin saturated in Na_2HPO_4 - citric acid buffer (i.e., pH 6, 8, 9.9, 10.8) were studied on mice skin (Hung et al., 2010). Increasing in lipophilicity (silychristin < silydianin < silybin) resulted in higher skin deposition and more compounds could permeate across the skin. The less ionized form (pH 8) showed more skin uptake with no skin irritation determined by transepidermal water loss (TEWL) and erythema index. In contrary, the skin permeation study of 2 %w/w silymarin microemulsion applied onto abdominal pig skin revealed no silymarin found in the receptor compartment, but small amount of silymarin found in the skin extract (Panapisal et al., 2012). Authors explained that high amount of surfactant/co-surfactant may dissolve and localize most of silymarin in the interfacial film than through the skin. On other word, silymarin showed high affinity to the system and may not permeate into the skin. To improve skin permeation, one of approaches may be lower down drug-system affinity by decreasing the amounts of surfactant and/or co-surfactant. Nanoemulsion is another emulsion system that has similar structure and compositions (oil, surfactant, water) as microemulsion, but lower surfactant content.

4. Nanoemulsion development for skin delivery

Various poorly soluble drugs have been employed in nanoemulsion formulations for skin delivery. For instance, retinyl palmitate (RP) nanoemulsion showed the highest encapsulation efficiency of 98.73 %, while liposome (LP) and solid lipid nanoparticle (SLN) were 68.02 % and 94.59 %, respectively (Clares et al., 2014). In addition, the cumulative amount of RP permeated through human skin (6.67 μg) was higher for nanoemulsion than that of LP (4.36 μg) and SLN (3.64 μg) at 38 hours. The flux of RP nanoemulsion (0.37 $\mu\text{g}/\text{h}$) was also significantly higher than that of SLN and LP (0.15 and 0.10 $\mu\text{g}/\text{h}$, respectively). Similarly, the cumulative amount of Coenzyme Q₁₀ (Q₁₀) released from nanoemulsion was higher than those from nanostructured lipid carriers (NLC) (Teeranachaideekul et al., 2007). In skin permeation study, the highest total amount of Q₁₀ was found in the receptor medium at 24 hours after applying Q₁₀-loaded nanoemulsion (Junyaprasert et al., 2009). High amount of Q₁₀ released from nanoemulsion could promote the penetration of Q₁₀ into the skin. Therefore, nanoemulsion is chosen as delivery system in this study due to its high entrapment efficiency, prolonged released and skin permeation enhancement.

Nanoemulsion is optically translucent to opaque flowable liquid due to its droplet size ranging between 20-200 nm (Gutiérrez et al., 2008). It is kinetically stable and non-equilibrium system. Formation of nanoemulsion can be both low-energy (e.g. phase inversion temperature method and spontaneous emulsification) and high-energy (e.g. ultrasonication and high-pressure homogenization (HPH)) methods. A comparative study of nanoemulsion preparation methods was reported. Rutin (RU) nanoemulsions were prepared using different techniques including spontaneous emulsification (SE) method and HPH method (Sharma et al., 2015). The particle size of RU nanoemulsion prepared by HPH method was significantly smaller and had

lower polydispersity index than that of nanoemulsion prepared by SE method. Moreover, RU nanoemulsion prepared by HPH method also showed greater % drug released at 6 hours. Therefore, HPH method was used in this study to produce good characteristics of nanoemulsions and it is ease for industrial scale up. The HPH production parameters including pressure, number of cycles, and temperature were reported to have an effect on particle size of nanoemulsions (Sharma et al., 2015; Wang et al., 2008; Yuan et al., 2008). Therefore, those production parameters were standardized.

In general, nanoemulsion consists of three main compositions namely oil, surfactant (and co-surfactant), and aqueous. Most cases, surfactants alone may insufficiently reduce the interfacial tension between oil and water to form small droplet (Talegaonkar and Negi, 2015). The addition of short to medium chain alcohols as co-surfactant can also reduce more oil/water interfacial tension. They locate between hydrocarbon tails of surfactant, which could stabilize the interfacial layer of nanoemulsion. Hence, surfactant and co-surfactant are considered as important parts, which can influence nanoemulsion formation in terms of particle size and stability. Surfactant/co-surfactant mixture (smix) ratios and concentrations were studied in nanoemulsion formulations (Hussain et al., 2016; Wooster, Golding and Sanguansri, 2008; Yuan et al., 2008), which the high amount of surfactant(s) showed smaller in particle size, narrow size distribution and better stability. However, the effect of smix ratio on particle size and stability were not inevitable and depended on types of oil, surfactant/co-surfactant, and also their proportions.

The selection of surfactant and co-surfactant is considered important. According to previous report (Woo et al., 2007), silymarin showed very high soluble in diethylene glycol monoethyl ether (Transcutol[®]; 350.1 mg/mL). Transcutol[®] is considered safe with low toxicity (Sullivan Jr et al., 2014), which is suitable for

pharmaceutical uses, especially topical application. Transcutol[®] was selected as a co-surfactant in this study to improve silymarin loading as well as its stability. Compositions of nanoemulsions containing Transcutol[®] are obtained from literatures. Non-ionic surfactants including Cremophor[®] RH40, Labrasol[®], Tween[®] 20 and Tween[®] 80 were considered because of their low irritation and high HLB value yielding oil in water nanoemulsion. In addition, solubilities of silymarin in these surfactants were ranking from Tween[®] 80 (35.4 mg/mL), Cremophor[®] RH40 (41.2 mg/mL), Labrasol[®] (79.8 mg/mL) and Tween[®] 20 (131.3 mg/mL) (Liu et al., 2007; Woo et al., 2007). Especially, these surfactants were previously used with Transcutol[®] in nanoemulsions (Alvarado et al., 2015; Dixit et al., 2008; Kumar et al., 2009; Tang et al., 2013). Increasing silymarin solubility was expected with helps of both surfactant and Transcutol[®], which Tween[®] 20 was selected due to its high solubility of silymarin.

In this study, oil-in-water nanoemulsions of different smix ratios and smix concentrations were prepared using high-pressure homogenization method in order to observe their effects on particle size, size distribution and physical stabilities. After that, silymarin nanoemulsions were studied on physical properties, physical stabilities and chemical stability. In addition, *in vitro* release of silymarin nanoemulsion and silymarin microemulsion (GL11, Panapisal et al. (2012)) were compared. The methods are described in Chapter 3.

CHAPTER 3

MATERIALS AND METHODS

Chemicals

Absolute ethanol, Analytical grade (Merck, Germany and RCI Labscan, Thailand)

Buffer solutions pH 4.01, 7.00, 9.21 (InLab[®] Solutions, Mettler-Toledo, USA)

Carbopol[®] 940 (Namsiang Trading Co., Ltd., Thailand)

Caprylic/capric triglyceride or Lexol[®] GT-865 (Namsiang Trading Co., Ltd., Thailand)

Caprylocaproyl polyoxyl-8 glycerides or Labrasol[®] (P.C. Intertrade Co., Ltd., Thailand)

Diethylene glycol monoethyl ether or Transcutol[®] CG (P.C. Intertrade Co., Ltd., Thailand)

Glycerol mono-oleate (Croda Co., Ltd., Thailand)

Hydroxypropyl methylcellulose (HPMC) E5 (Namsiang Trading Co., Ltd., Thailand)

Methanol, HPLC grade (Honeywell, Burdick and Jackson[®], Korea)

85 % Ortho-phosphoric acid, Analytical grade (Merck, Germany)

Potassium chloride (Merck, Germany)

Potassium dihydrogen orthophosphate, Analytical grade (Ajax Finechem, Australia)

Polyoxyethylene 20 sorbitan monolaurate or Tween[®] 20 (Namsiang Trading Co., Ltd., Thailand)

Polyoxyl 40 hydrogenated castor oil or Cremophor[®] RH40 (BASF, Germany)

Polyvinylpyrrolidone K90 or PVP K90 (Namsiang Trading Co., Ltd., Thailand)

Silibinin or Silybin (Sigma-Aldrich, Germany)

Silymarin (a gift from Berlin Pharmaceutical Industry Co., Ltd., Thailand)

Sodium chloride (Merck, Germany)

Sodium phosphate dibasic heptahydrate (Sigma-Aldrich, Germany)

Triethanolamine (Namsiang Trading Co., Ltd., Thailand)

Ultrapure water (produced by Maxima UF, Elga)

Apparatus

Analytical balance	(Model XP, Mettler-Toledo, USA)
Balance	(Model 1518B MP8-1, Sartorius, Germany)
High performance liquid chromatography	
Automatic sample injector	(Model SIL-10A, Shimadzu, Japan)
Column	(Phenomenex Luna C18, 5 μ m, 4.6 x 250 mm, USA)
Column oven	(Model CTO-10A, Shimadzu, Japan)
Degasser	(Model DGU-14A, Shimadzu, Japan)
Liquid chromatograph pump	(Model LC-10AD VP, Shimadzu, Japan)
Security guard column	(Phenomenex C18; ODS: Octadecyl, 4 x 3 mm, USA)
System controller	(Model SCL-10A VP, Shimadzu, Japan)
UV-VIS detector	(Model SPD-10A VP, Shimadzu, Japan)
High-pressure homogenizer	(Model Emulsiflex C5, Avestin, Canada)
High-speed homogenizer	(Model D-500, Wiggins, Germany)
High-speed refrigerated micro centrifuge	(Model MX-305, Tomy, Japan)
Hot air incubator	(Model BE-200, Memmert, USA)
Magnetic stirrer	(Model SLR, Schott, Germany)
Microliter pipettes	(Model Pipetman P20, P200 and P1000, Gilson, USA)
Modified Franz diffusion apparatus	
pH meter	(Model S220 Sevencompact, Mettler-Toledo, USA)
Refrigerator	(Model SJ-W36J-GY, Sharp, Thailand)
Ultracentrifuge	(Model L-80, Beckman Coulter, USA)
Ultrasonic bath	(Model Clifton MU-8, Nickel-Electro Ltd., UK)
UV-Visible spectrophotometer	(Model UV-1601, Shimadzu, Japan)
Vacuum pump	(Model DOA-V130-BN, Waters, USA)

Viscometer	(Model Programmable DV-II ⁺ , Brookfield, USA)
Vortex mixer	(Model Vortex-Genie 2, G560E, Scientific Industries, USA)
Zetasizer	(Model Nano ZS, Malvern, UK)

Materials

Disposable polystyrene cuvette, DTS0012	(Malvern, UK)
Injection vial	
Nylon membrane filter, 0.45 μ m	(Membrane Solutions, USA)
Parafilm® M	(Pechiney Plastic Packaging, Inc., USA)
Quartz cuvette, 10mm x 10mm	(Starna Scientific Ltd., UK)
Regenerated cellulose tubular membrane products, Inc., USA)	(CelluSep T4, Membrane filtration products, Inc., USA)
Scalp vein set, 21G x ¾”	(Nipro Corp., Japan)
Septa, PTFE/Silicone, 8mm x 0.045”	(Science Integration Co., Ltd., Thailand)
Stopper	
Syringe filter, PVDF, 13mm, 0.45 μ m	(Science Integration Co., Ltd., Thailand)
Syringe, 5 ml	(Nipro Corp., Ltd., Japan)
Thin wall – hypodermic needle, 18G x 1½”	(Nipro Corp., Ltd., Japan)
Ultracentrifuge tube, Polycarbonate bottle, 10.4 mL	(Beckman Coulter, USA)

Methods

A. Development and characterization of blank nanoemulsions

1. Preparation of blank nanoemulsions

Oil-in-water nanoemulsions were prepared by a modified high-pressure homogenization method (Wang et al., 2008). Firstly, ultrapure water was added into the mixture of caprylic/capric triglycerides (CCT), Tween[®] 20 and Transcutol[®] which were mixed using a magnetic stirrer for 30 minutes. Then, pre-emulsions were prepared using a high-speed homogenizer (D500, Wigger Hauser) at a speed of 22,000 rpm for 10 minutes. After that, they were further homogenized by a high-pressure homogenizer (Emulsiflex-C5) at pressure of 1,000 bar for six cycles. All processes were performed at room temperature.

2. Effects of smix ratio and smix concentration on physical properties and stabilities of blank nanoemulsions

Smix ratio and concentration were varied to obtain an optimum ratio and concentration that produced stable nanoemulsions (Table 1). Physical properties (Section C1.1 and C1.2) and physical stabilities including centrifugation (Section C2.1), heating-cooling cycles (Section C2.2), and room temperature (Section C2.3) were conducted with all nanoemulsions.

Table 1 Composition of blank nanoemulsions

Formulation	Smix ratio	Smix concentration (% w/w)	Composition (% w/w)		
			CCT	Tween [®] 20	Transcutol [®]
F1	1 : 0	10	10	10	-
F2	1 : 0.14	15	10	13	2
F3	1 : 0.25	15	10	12	3
F4	1 : 0.36	15	10	11	4
F5	1 : 0.5	15	10	10	5
F6	1 : 0.5	18	10	12	6
F7	1 : 0.5	21	10	14	7
F8	1 : 0.5	24	10	16	8
F9	1 : 0.5	30	10	20	10
F10	1 : 1	20	10	10	10
F11	1 : 1.5	25	10	10	15
F12	1 : 2	30	10	10	20

3. Stabilization of nanoemulsions using gelling agent

Gelling agents, which are Carbopol[®] 940, PVP K90 and HPMC E5, were gently added into the finished blank nanoemulsions and stirred with a magnetic stirrer at 300 rpm. For nanoemulsions containing Carbopol[®] 940, they were finally neutralized using triethanolamine to obtain target pH of 5-6. Various concentrations of each gelling agent were studied. Appearance (Section C1.1), particle size and size distribution of nanoemulsions (Section C1.2) during stored in heating-cooling cycles (Section C2.2) and at room temperature (Section C2.3), pH (Section C1.3), and viscosity (Section C1.4) were evaluated for their ability to help stabilize nanoemulsions.

Type and concentration of gelling agent which yielded the stable nanoemulsions were selected and used in the preparation of silymarin nanoemulsions.

B. Preparation of silymarin nanoemulsion

Various amounts of silymarin i.e., 0.5 %, 0.75 %, 1 %, 1.5 %, 2 % and 2.5 %w/w were incorporated into the selected nanoemulsions from Section A3, which were firstly performed on the formulation without gelling agent and then with gelling agent. Briefly, silymarin was dissolved in Tween[®] 20 or Transcutol[®] at 50 °C and then nanoemulsion was prepared with the same method as described in Section A1 and A3. Silymarin nanoemulsions were evaluated by which of the following: physical properties (Section C1), physical stabilities (Section C2), chemical stability (Section C3) and *in vitro* release study (Section C4).

C. Characterization of blank and silymarin nanoemulsions

1. Physical properties

1.1 Appearance

After 24 hours of preparation, nanoemulsions were evaluated in terms of phase separation and creaming. In addition for silymarin nanoemulsions, drug precipitation were evaluated by visual inspection.

1.2 Particle size and size distribution

Particle size and size distribution were analyzed using dynamic light scattering (Zetasizer Nano ZS, Malvern) at a scattering angle of 173° using a 633 nm laser. Nanoemulsion was diluted with ultrapure water (1:100, v/v) to avoid multiple scattering. Sample was measured after 10 seconds of equilibration at 25 °C and the results were reported as the average of three measurements and standard deviation. Size measurement was modified from Wooster et al. (2008).

1.3 pH measurement

pH meter was used to measure the formulation pH and buffer solutions of pH 4.01, 7.00 and 9.21 were used to calibrate the instrument. All measurements were performed at 25 °C.

1.4 Viscosity

Brookfield rheometer was used to determine the formulation viscosity with a small sample adapter (SSA; code S00). Twenty grams of the sample was used without dilution. Shear rate was varied from 10 to 200 rpm and all measurements were performed at 25 °C.

1.5 Entrapment efficiency

The entrapment efficiency (EE) of silymarin in nanoemulsion was investigated by ultracentrifugation method using 60,000 rpm for 1 hour at 25 °C. Silymarin in both phases were analyzed using a validated UV-Vis spectrophotometric method described in Section E. % EE was calculated by Equation 1.

$$\%EE = [W_E / (W_E + W_F)] \times 100$$

Equation 1 Percentage Entrapment efficiency

W_E = Total amount of silymarin entrapped in the nanoemulsion

W_F = Total amount of free silymarin in the water layer

1.6 Drug content

0.5 g of silymarin nanoemulsion were extracted by methanol and analyzed using a validated HPLC method (Section D). Silymarin content in nanoemulsion should be $\pm 10\%$ of the theoretical concentration.

2. Physical stabilities

2.1 Preliminary physical stability screening by centrifugation

Nanoemulsions were centrifuged at 3,500 rpm for 30 minutes at 25 °C (Kumar et al., 2009). Any phase separation or instability was evaluated.

2.2 Heating-cooling cycles

Nanoemulsions, which remained no change after centrifugation and had particle size between 20-200 nm, were kept in the refrigerator at 4 °C for 48 hours and in the hot air oven at 45 °C for 48 hours per one cycle. The test was carried out for six cycles (Panapisal et al., 2012). At the end of each cycle, measurements of particle size and size distribution were performed in triplicate. Any phase separation or instability was evaluated.

2.3 Room temperature

Nanoemulsions, which were performed in heating-cooling cycles (Section C2.2), were also kept in the same period of time at room temperature. Particle size of the sample was measured as a function of time at 25 °C using dynamic light scattering same as mentioned in Section C1.2. At each time point, sample was diluted 1:100 v/v with ultrapure water which did not affect the assessment of the Ostwald ripening rate. The Ostwald ripening rate (ω) was obtained from the slope of r^3 versus time explained by LSW theory and referred to Equation 2 (Wooster et al., 2008).

$$\omega = \frac{dr_N^3}{dt}$$

Equation 2 Ostwald ripening rate

where ω = ostwald ripening rate (nm³/h)

r = particle size of nanoemulsion in radius diameter (nm)

t = time (hour)

3. Chemical stability

Silymarin nanoemulsion, which remained the most stable in physical stability studies, was stored in amber glass bottles at 40 °C for 3 months. Quantifications of silymarin were performed at 0, 1, 2 and 3 months using a validated HPLC method described in Section D. No more than 10 % drug loss was considered that the silymarin nanoemulsion was chemically stable. The method is modified from Panapisal et al. (2012).

4. *In vitro* release study

4.1 Preparation of silymarin solution

Firstly, 0.5 % w/w of silymarin was dissolved in ethanol and then mixed with phosphate buffer saline (PBS) to obtain final concentration of 40 %w/w ethanol in PBS on a magnetic stirrer for 10 minutes.

4.2 Preparation of silymarin microemulsion

The silymarin microemulsion (GL11) was selected and the method of preparation was followed from Panapisal et al. (2012). 0.5 %w/w of silymarin was added into a mixture of 25 %w/w Labrasol[®] and Cremophor[®] RH40 (1:1), 25 %w/w Transcutol[®], and 6 %w/w glycerol mono-oleate at 50 °C. After the silymarin dissolved, 43.5 %w/w of ultrapure water was added and stirred for 10 minutes.

Release studies of silymarin solution, silymarin nanoemulsion, and silymarin microemulsion were performed and compared using modified Franz diffusion cells, referring to the method of Panapisal et al. (2012). The cellulose membrane (cut-off molecular weight of 12,000-14,000) was first hydrated in ultrapure water for 24 hours, then washed by hot water, and soaked in receptor solution for 1 hour before the experiment. Then, the membrane was clamped between the donor and the receptor

compartments of the cell. The receptor solution was 40 % ethanol in phosphate buffer saline pH 7.4, and it was maintained at 37 °C using a thermostatic water bath and magnetically stirred at 600 rpm throughout the experiment. The receptor solution and membrane was equilibrated to the desired temperature for 1 hour before the experiment. After equilibration, 0.250 g of the test sample was transferred into the donor compartment, and then covered with paraffin film to prevent evaporation. Five milliliters of receptor solution were withdrawn at 0.5, 1, 2, 3, 4, 6, 8, 10, 12, 16, 20, 24 hours from receptor compartment, and then replaced by a fresh medium in equal amount taken. The samples were analyzed for silymarin using a validated UV-Vis spectrophotometric method described in Section E. Three replicates of each experiment were performed.



D. Quantitative analysis of silymarin by high performance liquid chromatographic (HPLC) method

The analysis was subjected to use in drug content (Section C1.6) and chemical stability (Section C3) of silymarin nanoemulsion.

1. The conditions were modified from Panapisal et al. (2012) as follows;

Column : Phenomenex Luna C18 (5 μ m, 4.6 x 250 mm)

Mobile phase : Solution A (water : methanol : phosphoric acid, 80:20:0.5)

Solution B (methanol : water : phosphoric acid, 80:20:0.5)

Solution A and B were prepared, filtered through 0.45 μ m membranes and degassed by sonication for 30 minutes.

Injection volume : 10 μ L

Flow rate : 1 mL/minute

Temperature : 40 $^{\circ}$ C

Detector : UV-Visible spectroscopy at wavelength 288 nm

Gradient systems :

Time (min)	Solution A (%)	Solution B (%)	Elution
0-5	85	15	Isocratic
5-20	85 --> 55	15 --> 45	Linear gradient
20-40	55	45	Isocratic
40-41	55 --> 85	45 --> 15	Linear gradient
41-60	85	15	Equilibration

2. Standard solution preparation

2.1 Silybin was accurately weighed and dissolved in ethanol. Then, this stock solution was diluted with 30 % ethanol in phosphate buffer saline pH 7.4 to obtain final concentrations in the range of 2-20 $\mu\text{g/mL}$.

2.2 Silymarin was accurately weighed and dissolved in ethanol. Then, this stock solution was diluted with 30 % ethanol in phosphate buffer saline pH 7.4 to obtain final concentrations in the range of 6-60 $\mu\text{g/mL}$.

3. HPLC sample preparation

Briefly, 0.5 g of blank nanoemulsions or silymarin nanoemulsions was dissolved with ethanol. This solution was further diluted with ethanol to 1:5 v/v and filtered through a PVDF filter.

4. Validation of HPLC method

The analysis was validated with typical parameters, which were specificity, linearity, accuracy, precision, limit of detection, and limit of quantitation.

4.1 Specificity

The specificity of HPLC method was involved demonstration of the discrimination of silybin or silymarin in the presence of excipients (blank nanoemulsion(s) and receptor solution). This could be done by spiking silybin or silymarin with appropriate levels of excipients and demonstrating that the response was unaffected by the presence of these excipients.

4.2 Linearity

Six concentrations of silybin or silymarin solutions were prepared and analyzed. Silybin A and silybin B were reference peaks for silymarin quantification and the sum of their peak areas were calculated. The linear regression was

calculated by plotting the relationship between silybin or silymarin concentrations and peak areas. The linearity was determined from the coefficient of determination ($r^2 \geq 0.9990$). The test was done in triplicates.

4.3 Accuracy

Three concentrations of silymarin solution (five replications per concentration), covering the linearity range, were prepared and analyzed. The percentage of recovery should be in the range of 90-110 %.

4.4 Precision

a) Repeatability

Three concentrations of silymarin solution (five replications per concentration), covering the linearity range, were prepared and analyzed in the same run. The precision of each concentration was determined from the percentage of coefficient of variation (% CV). The CV should be less than 5 %.

b) Intermediate precision

Three concentrations of silymarin solution covering linearity range were prepared and analyzed in five different runs. The precision of each concentration was determined from the percentage of coefficient of variation (% CV). The CV should be less than 5 %.

4.5 Limit of detection (LOD)

The limit of detection of HPLC method is the lowest concentration of silybin which could be detected qualitatively. LOD calculation is based on the standard deviation of the response and the slope of standard curve (Equation 3).

$$LOD = \frac{3.3\sigma}{S}$$

Equation 3 Limit of detection

where σ = the standard deviation of the response

S = the slope of the calibration curve

4.6 Limit of quantitation (LOQ)

The limit of quantitation of HPLC method is the lowest concentration of standard at that level could be quantitated with acceptable accuracy and precision. LOQ calculation is based on the standard deviation of the response and the slope of standard curve (Equation 4).

$$LOQ = \frac{10\sigma}{S}$$

Equation 4 Limit of quantitation

where σ = the standard deviation of the response

S = the slope of the calibration curve



E. Quantitative analysis of silymarin by UV-Vis spectrophotometric method

The analysis was subjected to use in entrapment efficiency (Section C1.5) and release studies (Section C4).

1. Standard solution preparation

1.1 Entrapment efficiency

Silymarin was accurately weighed and dissolved in methanol. Then, this stock solution was sonicated for 10 minutes and diluted with methanol to obtain final concentrations in the range of 4-20 µg/mL.

1.2 Release studies

Silymarin was accurately weighed and dissolved in ethanol. Then, this stock solution was sonicated for 10 minutes and diluted with 40 % ethanol in phosphate buffer saline pH 7.4 to obtain final concentrations in the range of 4-25 µg/mL.

2. UV-Vis spectrophotometric sample preparation

2.1 Entrapment efficiency

Blank nanoemulsion or silymarin nanoemulsion was accurately weighed and dissolved in methanol. Then, these stock solutions were sonicated for 10 minutes and diluted with methanol.

2.2 Release studies

Blank nanoemulsion or silymarin nanoemulsion was accurately weighed and dissolved in ethanol. Then, these stock solutions were sonicated for 10 minutes and diluted with 40 % ethanol in phosphate buffer saline pH 7.4.

Receptor solutions, which were taken from the release studies at each point of time, were diluted with 40 % ethanol in phosphate buffer saline pH 7.4.

3. Validation of UV-Vis spectrophotometric method

The analysis was validated with typical parameters, which were specificity, linearity, accuracy and precision.

3.1 Specificity

The specificity of UV-Vis spectrophotometric method was involved demonstration of the discrimination of silymarin in the presence of excipients of blank nanoemulsion. This could be done by spiking silymarin with appropriate levels of excipients and demonstrating that the response at the analytical wavelength was unaffected by the presence of these excipients.

3.2 Linearity

Six concentrations of silymarin solutions were prepared and analyzed. The linear regression was calculated by plotting the relationship between silymarin concentrations and absorbance at 288 nm. The linearity was determined from the coefficient of determination ($r^2 \geq 0.9990$). The test was done in triplicates.

3.3 Accuracy

Three concentrations of silymarin solution (five replications per concentration), covering the linearity range, were prepared and analyzed. The percentage of recovery was in the range of 97-103 %.

3.4 Precision

a) Repeatability

Three concentrations of silymarin solution (five replications per concentration), covering the linearity range, were prepared and analyzed in the same run. The precision of each concentration was determined from the percentage of coefficient of variation (% CV).

b) Intermediate precision

Three concentrations of silymarin solution covering linearity range were prepared and analyzed in five different runs. The precision of each concentration was determined from the percentage of coefficient of variation (% CV).

F. Statistical analysis

All data were reported as mean \pm standard deviation.



CHAPTER 4

RESULTS AND DISCUSSION

A. Development and characterization of blank nanoemulsions

1. Development of blank nanoemulsions

Oil-in-water nanoemulsions were successfully prepared by high-pressure homogenization method using caprylic/capric triglycerides (CCT) as an oil phase, ultrapure water as an aqueous phase, Tween[®] 20 as a surfactant and Transcutol[®] as a co-surfactant. Surfactant and co-surfactant mixture (smix) ratios were varied (i.e., 1:0, 1:0.14, 1:0.25, 1:0.36, 1:0.5, 1:1, 1:1.5, and 1:2) with different concentrations in the range of 10 % to 30 % smix (Table 1). The physical appearances of all freshly prepared nanoemulsions were opaque white liquid with low viscosity (Figure 3), they had no creaming or phase separation after 24 hours of preparation.



Figure 3 Physical appearances of (a) freshly prepared blank nanoemulsion F1 and (b) freshly prepared blank nanoemulsions F1, F5, F10 and F11 from left to right, respectively.

As shown in Table 2, the mean particle sizes (z-average) of blank nanoemulsions were in the range of 88.3 to 227.2 nm. The F12 formulation containing the most amount of Transcutol[®] showed oversized particles (>200 nm) and was excluded for the further studies. All formulations had narrow size distribution and uniform size with very low values of polydispersity index (0.086-0.197), which was an advantage of using high pressure homogenizer.

Table 2 Physical properties and stabilities of blank nanoemulsions

Formulation	Smix ratio	Smix conc. (% w/w)	Size (nm) ^a	Pdl ^a	Physical stability studies		
					Cent. ^b	HC cycle ^c	ω (nm ³ /h)
F1	1 : 0	10	113.8 ± 0.17	0.152 ± 0.01	uc	5 cycles	368.24
F2	1 : 0.14	15	96.0 ± 1.48	0.171 ± 0.01	uc	2 cycles	797.37
F3	1 : 0.25	15	90.8 ± 2.49	0.153 ± 0.01	uc	2 cycles	908.32
F4	1 : 0.36	15	106.0 ± 1.36	0.157 ± 0.01	uc	3 cycles	883.24
F5	1 : 0.5	15	119.8 ± 1.07	0.168 ± 0.01	uc	3 cycles	980.58
F6	1 : 0.5	18	91.2 ± 0.68	0.197 ± 0.01	uc	1 cycle	N/A
F7	1 : 0.5	21	89.6 ± 0.17	0.188 ± 0.11	c	N/A	N/A
F8	1 : 0.5	24	88.3 ± 1.13	0.161 ± 0.01	c	N/A	N/A
F9	1 : 0.5	30	102.2 ± 0.70	0.091 ± 0.01	c	N/A	N/A
F10	1 : 1	20	118.5 ± 1.82	0.147 ± 0.00	uc	1 cycle	2508.5
F11	1 : 1.5	25	148.7 ± 0.59	0.086 ± 0.01	uc	1 cycle	8716.7
F12	1 : 2	30	227.2 ± 0.70	0.109 ± 0.02	c	N/A	N/A

^a reported as mean ± SD, n=3

^b Cent. = centrifugation, uc: unchanged, c: creaming

^c HC Cycle, heating-cooling cycle, reported as the number of stable cycle(s)

ω : Ostwald ripening rate

Nanoemulsions were centrifuged at low speed which their kinetic stability was accelerated by gravity force. Separation of the disperse phase from emulsion or creaming may be induced by the centrifugation. For o/w emulsion and oil with a density less than water, a rising of the cream was observed. Stokes' law could be used to explain these instabilities of emulsion where creaming rate is influenced by particle size, viscosity, and densities of internal and external phases as showed in Equation 5. The results showed that most nanoemulsions showed no change after centrifugation (Figure 4), except four formulations containing smix ratio of 1:0.5 and high smix concentration (F7, F8, F9), and high transcuto[®] (F12) which showed creaming and were eliminated. Therefore, other nanoemulsions were further accelerated by temperature.

$$V = \frac{2r^2(\rho_1 - \rho_2)g}{9\eta}$$

Equation 5 Stokes' Law

where, V is the creaming rate (cm/s), r is the particle radius (cm), $(\rho_1 - \rho_2)$ is the difference in density between of internal phase and external phase, g is the gravitational constant; 981 cm/s^2 and η is the viscosity of external phase

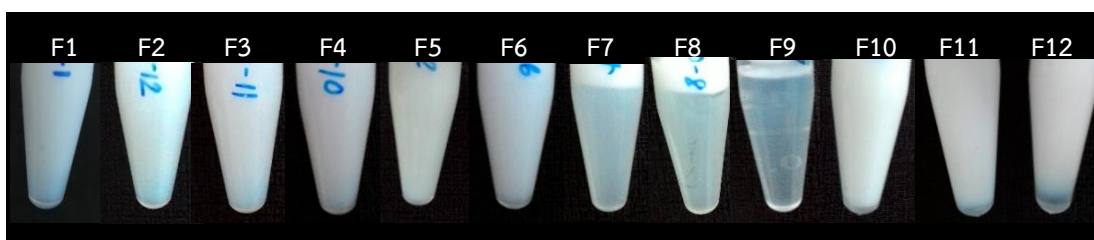


Figure 4 Physical appearances of blank nanoemulsions after centrifugation

The heating-cooling cycle stability tests of nanoemulsions were determined by observing their physical appearances and also the growth of particle size at the end of each cycle. The results showed that mean particle sizes of all formulations

increased after the first cycle of the test and creaming was occurred when the mean particle size exceeded 200 nm (data shown in Appendix A). Nanoemulsion F1 that contained only Tween[®] 20 without Transcutol[®] revealed the most stable formulation and passed through 5 cycles of heating-cooling (Table 2).

Nanoemulsions were stored at room temperature and their particle sizes were measured at the same time point of heating-cooling cycle. The Ostwald ripening rates were calculated from linear regression of the slope of r^3 versus time plot (Appendix A) as shown in Table 2. The most stable nanoemulsion, F1, showed the lowest Ostwald ripening rate of 368.24 nm³/h, while the formulation (F11) containing high amount of Transcutol[®] as well as high smix concentration of 25 % showed the highest Ostwald ripening rate of 8716.7 nm³/h.

2. Effects of smix ratio and smix concentration on physical properties and stabilities of blank nanoemulsions

At a constant smix ratio of 1:0.5 (F5-F9), increasing the concentration of smix resulted in particle size reduction, except formulation F9. The results were consistent with the study of Yuan et al. (2008), that increasing surfactant concentration resulted in size reduction. Smaller particle sizes may require more surfactant to be adsorbed at the interfacial film because of larger surface area. Their studies showed that the smallest size was obtained when 10 % w/w Tween[®] 20 was used. Among this smix ratio of 1:0.5 formulations, the higher smix concentration (>20 %; F7, F8, F9 in Table 2) showed poorer stability in centrifugation study. The least smix concentration (F5) revealed more stable than other smix ratios of 1:0.5 formulations in heating-cooling cycle. This may imply that a small particle size and high concentration of surfactant did not always yield more stable nanoemulsion. As previous reports (McClements (1994); Uluata, Decker and McClements (2016)), nanoemulsion also showed creaming instability at higher surfactant concentration.

It could be explained that non-adsorbed surfactant could form micelles in aqueous phase and promote depletion flocculation (or droplet aggregation). Those micelles could generate an osmotic attraction between oil droplets. The number of free surfactant micelles in the aqueous phase increased and overall attractive forces (Van der Waals and osmotic) became large enough to overcome the overall repulsive forces (electrostatic) leading to depletion flocculation. Therefore, an optimum smix concentration should take into consideration at specific smix ratio.

At a constant smix concentration of 15 % (F2-F5), increasing the proportion of Transcutol[®] resulted in larger particle size. In heating-cooling cycle, F2 and F3 formulations, which contain 13 % and 12 % Tween[®] 20, respectively, revealed less stable when compared with F4 and F5 (Table 2). In addition, the amount of Tween[®] 20 was fixed at 10 % where increasing in Transcutol[®] (i.e., F1; 0 %, F5; 5 %, F10; 10 %, F11; 15 % and F12; 20 %) larger particle sizes were obtained same as mentioned above.

Heating-cooling cycle showed the results in corresponding to Ostwald ripening rates, where the higher rate showed less stable formulation in heating-cooling cycle. An excess surfactant in aqueous phase could form micelles, which could then dissolve and transport oil to other oil droplets causing Ostwald ripening (Wooster et al., 2008). In addition, solubility of oil in aqueous phase also has major influence on physical stability of nanoemulsion, with Ostwald ripening rates are proportional to the molecular volume of oil. However, triglyceride oils (i.e., CCT) are considered insoluble in water and could act as a kinetic barrier to Ostwald ripening. In conclusion, surfactant and co-surfactant was believed to play an important role in contributing to unstable nanoemulsions for this study. Transcutol[®] also seemed to have a negative effect on nanoemulsion stability, which may cause by imperfect surfactant/co-surfactant film formation due to its properties as good co-solvent and hygroscopic liquid (Sullivan Jr et al., 2014).

The formulation containing high proportion of Transcutol[®] was preferred to consequently achieve high drug loading. However, only formulations that passed physical stability studies were chosen which are blank nanoemulsion F4 and F5. Therefore, blank nanoemulsions, F1, F4 and F5, were chosen for further development due to they remained the most stable systems in heating-cooling studies.

3. Stabilization of nanoemulsions using gelling agent

Even though F1, F4, and F5 were considered the most stable formulations in heating-cooling studies, it would be desirable to increase the stability of nanoemulsions by incorporating some stabilizer. Increasing viscosity of continuous phase is one of approach to delay internal droplet fusion referred to the stokes' law equation.

Various amounts of gelling agents were preliminarily incorporated into blank nanoemulsions F4 and F5 as shown in Table 3. Minimum and maximum concentration of each gelling agents were defined to obtain flowable nanoemulsions and better physical stability as details shown in Table 3.

The results showed that all gelling agents did not alter size and size distribution of blank nanoemulsions without gelling agent at day 0. After 3 days of storage at room temperature, F4 and F5 with 0.25 % and 0.50 % HPMC E5 showed creaming and were excluded from the experiment. All blank nanoemulsions with PVP K90 (0.10 %, 0.25 % and 0.50 %) also showed creaming after 3 days. Higher sized growth or instable blank nanoemulsions in case of 0.25 %, 0.5 % HPMC E5 and PVP K90 were found after adding gelling agents.

Table 3 Size and size distribution of blank nanoemulsions with gelling agents

Gelling agents (%w/w)	F4				F5				
	Day 0		Day 7		Day 0		Day 7		
	Size(nm)	Pdl	Size(nm)	Pdl	Size(nm)	Pdl	Size(nm)	Pdl	
0	103.7	0.185	129.3	0.105	100.0	0.173	130.1	0.109	
Carbopol [®] 940									
0.15	104.1	0.169	137.9	0.128	103.5	0.176	136.5	0.087	
0.175	105.2	0.170	135.7	0.105	103.6	0.170	137.7	0.124	
0.20	104.9	0.168	137.1	0.098	104.7	0.186	143.4	0.121	
HPMC E5									
0.10	102.9	0.174	135.7	0.129	102.6	0.166	133.0	0.082	
0.25	103.3	0.150	N/A	N/A	102.2	0.154	N/A	N/A	
0.50	99.9	0.177	N/A	N/A	99.2	0.169	N/A	N/A	
PVP K90									
0.10	103.6	0.178	N/A	N/A	102.7	0.159	N/A	N/A	
0.25	104.7	0.193	N/A	N/A	103.1	0.174	N/A	N/A	
0.50	103.7	0.169	N/A	N/A	102.53	0.168	N/A	N/A	

Table 4 showed that most blank nanoemulsions with or without gelling agent had acidic pH of ~ 3 except those with Carbopol[®] 940 due to final neutralization. Increase in gelling agent concentration showed slightly increase in viscosity for HPMC E5 and PVP K90. Whereas, nanoemulsions with Carbopol[®] 940 showed dramatically increase in viscosity with higher concentration of Carbopol[®] 940.

According to the stokes' law, higher viscosity could be more stable emulsion, the results showed that Carbopol[®] 940 could help improve nanoemulsions stability that showed no change after 7 days storage. Interestingly, HPMC E5 was reported to act as a polymeric emulsifier and could adsorb at liquid interface and also lower the interfacial tension (Wollenweber et al., 2000). The adsorption of polymer on the interfacial layer may be described according to train-loop-tail model which the hydrophobic parts formed trains and separated from loops and tails of hydrophilic parts in aqueous phase. The ratio of train, loop and tail parts

or HPMC grade could affect emulsion stability. In this study, HPMC E5 at 0.25 and 0.5 %w/w may unfortunately form train-loop-tail and result in aggregation between droplets leading to creaming of nanoemulsion. PVP K90 might have the same behavior or other unknown negative effect on nanoemulsions stability.

Then, the formulations, which remained no physical appearance change after 7 days at room temperature, were undergone heating-cooling cycle test (Table 5).

Table 4 pH and viscosity of blank nanoemulsions with gelling agents

Gelling agents (%w/w)	F4		F5	
	pH	Viscosity (cP)	pH	Viscosity (cP)
0	3.23	3.15	3.16	3.09
Carbopol [®] 940				
0.15	5.53	18.90	5.02	12.60
0.175	5.57	29.60	5.27	19.60
0.20	5.94	55.40	5.57	34.20
HPMC E5				
0.10	3.25	3.70	3.12	3.76
0.25	3.23	4.36	3.12	4.16
0.50	3.25	6.03	3.12	5.91
PVP K90				
0.10	3.23	3.66	3.16	3.46
0.25	3.23	2.86	3.13	4.09
0.50	3.24	3.94	3.13	5.76

At 0.2 %w/w Carbopol[®] 940, showed the most stable system in heating-cooling tests of nanoemulsion F4 and F5 (Table 5); therefore, it was selected for the further study with nanoemulsion F1 which also passed all six cycles. Although, it could improve physical stability in heating-cooling cycles, Ostwald ripening rate could not slow down by adding gelling agent. In contrast, 0.1 %w/w HPMC E5 of nanoemulsion F4 and F5 could not maintain nanoemulsion

system through six cycles, their Ostwald ripening rates were lower than that of blank nanoemulsions without HPMC E5.

0.2 %w/w Carbopol[®] 940 of nanoemulsion F5 were selected to load with silymarin because the formulation F5 contained higher proportion of Transcutol[®] when compared with F4, although they gave the same physical stabilities including heating-cooling cycles and Ostwald ripening rates. Moreover, 0.2 %w/w Carbopol[®] 940 of nanoemulsion F1 was also chosen for the further studies because the formulation did not contain Transcutol[®] in order to compare with F5.

Table 5 Physical properties and stabilities of blank nanoemulsions with gelling agents

Formulation / Gelling agent (%w/w)	Day 0		HC cycle ^b	ω (nm ³ /h)
	Size (nm) ^a	Pdl ^a		
F1				
C 0.20	117.7 ± 0.45	0.203 ± 0.01	6	398.72
F4				
C 0.15	105.9 ± 0.89	0.172 ± 0.00	3	950.13
C 0.175	104.9 ± 1.16	0.186 ± 0.01	3	941.89
C 0.20	105.7 ± 1.11	0.179 ± 0.00	4	975.02
H 0.10	105.2 ± 1.02	0.175 ± 0.00	2	862.25
F5				
C 0.15	101.0 ± 0.46	0.187 ± 0.02	3	1004.9
C 0.175	103.0 ± 0.46	0.174 ± 0.03	3	992.11
C 0.20	102.7 ± 1.10	0.186 ± 0.01	4	1033.2
H 0.10	101.9 ± 0.90	0.166 ± 0.01	2	915.23

C: Carbopol[®] 940, H: HPMC E5

^a reported as mean ± SD, n=3

^b HC Cycle, heating-cooling cycle, reported as the number of stable cycle(s)

ω : Ostwald ripening rate

B. Preparation of silymarin nanoemulsion

The appearance of silymarin extract is yellow powder. Since it is poorly water-soluble, it was firstly dissolved in Tween[®] 20 for F1 or in Transcutol[®] for F5 and heating at 50 °C. Then, remaining surfactant for F5, CCT and ultrapure water were added into the mixture, respectively.

0.5 %, 0.75 %, 1 % and 1.5 %w/w silymarin were successfully incorporated into blank nanoemulsion (F1). Their physical appearances were opaque-pale yellow liquid, which showed no creaming or unchanged over 24 hours after preparation. After centrifugation, only 1.5 %w/w silymarin showed creaming (Figure 5) and was excluded from the experiment. At higher concentration of silymarin resulted in larger particle size and tended to have poorer physical stabilities (Table 6). As can be seen in heating-cooling cycles (Table 6 and Figure 6b), 0.75 % and 1 %w/w silymarin could not pass at the first cycle which corresponded to their Ostwald ripening rates. It was clear that at high concentration of silymarin (i.e., 0.75 % and 1 %w/w), nanoemulsions were severely broken into two phases.



Figure 5 Physical appearances of 0.5 %, 0.75 %, 1 %, 1.5 %w/w silymarin nanoemulsions (F1) after centrifugation from left to right, respectively.

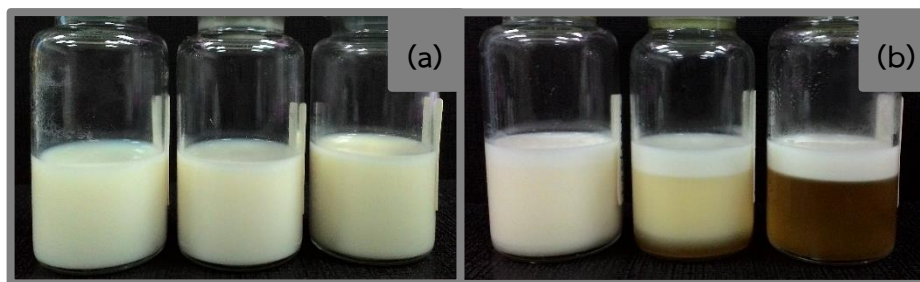


Figure 6 Physical appearances of (a) freshly prepared 0.5 %, 0.75 % and 1 %w/w silymarin nanoemulsions (F1) from left to right respectively. (b) Physical appearances of 0.5 %, 0.75 % and 1 %w/w silymarin nanoemulsions (F1) after one cycle of heating-cooling cycles.

Table 6 Physical properties and physical stabilities of silymarin nanoemulsions

Formulation/ Silymarin (%w/w)	Size (nm) ^a	Pdl ^a	Physical stability studies		
			Cent. ^b	HC cycle ^c	ω (nm ³ /h)
F1					
SM-0.5	109.9 ± 0.45	0.177 ± 0.01	uc	2 cycles	915.49
SM-0.75	113.0 ± 1.20	0.159 ± 0.01	uc	0 cycle	3008.4
SM-1	127.4 ± 1.74	0.064 ± 0.01	uc	0 cycle	41275
SM-1.5	578.6 ± 12.1	0.123 ± 0.04	c	N/A	N/A
F5					
SM-0.5	112.5 ± 0.56	0.141 ± 0.03	uc	1 cycle	5934.2
SM-0.75	119.8 ± 1.90	0.118 ± 0.00	uc	0 cycle	52830
SM-1*	207.2 ± 1.95	0.093 ± 0.03	uc	N/A	N/A
SM-1.5	N/A	N/A	N/A	N/A	N/A
SM-2	N/A	N/A	N/A	N/A	N/A
SM-2.5	N/A	N/A	N/A	N/A	N/A

^a Data of freshly prepared nanoemulsion; reported as mean ± SD, n=3

^b Cent. : centrifugation, uc: unchanged, c: creaming

^c HC Cycle, heating-cooling cycle, reported as the number of stable cycle(s)

ω : Ostwald ripening rate

* showed creaming after two days of preparation

0.5 %, 0.75 % and 1 %w/w silymarin were also successfully incorporated into blank nanoemulsion (F5). Although, higher concentrations of silymarin (i.g., 1.5 %, 2 % and 2.5 %w/w) were completely dissolved in Transcutol[®] but when the mixtures were processed through the method forming pre-emulsion by magnetic stirrer, the mixtures were then broken up and silymarin was then precipitated within 5 minutes. Since, solubility of silymarin in Transcutol[®], Tween[®] 20 and in CCT (Miglyol[®] 812) were 350.1, 131.3 and 0.8 mg/mL respectively reported by Woo et al. (2007). High solubility of silymarin in Transcutol[®] may cause more silymarin to solubilize in the external phase containing Transcutol[®] and water which could be observed by the color of the external phase. Transfer of both silymarin and Transcutol[®] to the external phase may lead to imperfect surfactant/co-surfactant interfacial film, larger particle size and unstable system. Additional study using Transcutol[®] as edge activator of minoxidil elastic vesicles which Transcutol[®] improved elasticity of the vesicular membrane (Mura et al., 2011). However, high concentration of Transcutol[®] could cause more drug dissolved in the external phase not remaining in the bilayer and resulting in a loss of elasticity.

The appearances of silymarin nanoemulsions F5 (Figure 7) were opaque-pale yellow liquid and had darker shade than F1 formulation loaded silymarin. No separation or creaming after 24 hours of preparation and after centrifugation was observed. After two days of preparation, only 1 %w/w silymarin nanoemulsion (F5) showed creaming; therefore, it was excluded from the experiment. Same particle size increase was observed with increasing silymarin concentration in agreement with nanoemulsions F1 loaded silymarin. Larger particle sizes appeared to have poorer physical stabilities of nanoemulsions.



Figure 7 Physical appearances of 0.5 %, 0.75 %, 1 %w/w silymarin nanoemulsions (F5) after centrifugation from left to right, respectively

At a constant concentration of 0.5 %w/w silymarin of nanoemulsion F1 and F5, their particle size were comparable (F1; 109.9 nm, F5; 112.5 nm) and did not differ much from their blank nanoemulsions (F1; 113.8 nm, F5; 119.8 nm). However, 0.5 %w/w silymarin (F5) showed much less physical stabilities than that of F1, which showed approximately 6 times higher rate of Ostwald ripening (Table 6).

At a constant concentration of 0.75 % silymarin of nanoemulsions F1 and F5, similar particle sizes were found compared with blank formulations and both formulations failed the first heating-cooling cycle. As can be seen in Table 5, Ostwald ripening rate of 0.75 % silymarin nanoemulsion (F5) showed extremely higher than that of F1 formulation. It may imply that Transcutol[®] had a negative effect on stability of nanoemulsions. Similarly, high amount of silymarin could cause instability of nanoemulsions which may due to large molecule flavonolignans in silymarin. As already known, silymarin could dissolve more in surfactant and may position in the surfactant/co-surfactant film. According to the interfacial film theory, the thin film of emulsifying agents may be overloaded by high quantity of silymarin.

Therefore, nanoemulsions F1 loaded with 0.5 %w/w and 0.75 %w/w silymarin were selected to increase their viscosities by adding 0.2 %w/w Carbopol[®] 940 referred to the results in Section A3.

The physical appearances of freshly prepared 0.5 % and 0.75 % w/w silymarin nanoemulsions F1 with 0.2 %w/w Carbopol[®] 940 were shown in Figure 8a. Their viscosities were comparable to blank nanoemulsion F1 with 0.2 %w/w Carbopol[®] 940. The particle sizes and size distribution did not alter from the formulation without gelling agent (Table 6 and 7). Although, nanoemulsion loaded with 0.5 % w/w presented sized-growth when stored at room temperature, this nanoemulsion passed six heating-cooling cycles. From this study, 0.5 %w/w silymarin nanoemulsion F1 with 0.2 %w/w Carbopol[®] 940 was selected due to its better stability outcomes than that of 0.75 %w/w silymarin nanoemulsion F1 with 0.2 %w/w Carbopol[®] 940. As seen in Figure 8b, 0.75 %w/w silymarin after the sixth cycle of heating-cooling test showed darker color and some creaming.

Silymarin nanoemulsion gel (SMNE gel), which is nanoemulsion F1 loaded 0.5 %w/w silymarin and 0.2 %w/w Carbopol[®] 940, was chosen to determine drug entrapment efficiency, drug content, chemical stability and *in vitro* release study.

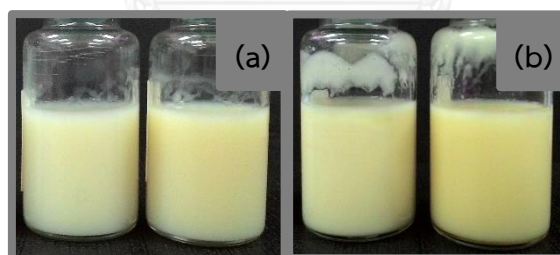


Figure 8 (a) Physical appearances of freshly prepared 0.5 %w/w (left) and 0.75 %w/w (right) silymarin nanoemulsions (F1) with 0.2 %w/w Carbopol[®] 940. (b) Physical appearances of 0.5 %w/w (left) and 0.75 %w/w (right) silymarin nanoemulsions (F1) with 0.2 %w/w Carbopol[®] 940 after stored for six cycles of heating-cooling cycles.

Table 7 Physical properties and physical stabilities of silymarin nanoemulsions (F1) with 0.2 %w/w Carbopol[®] 940

Formulation/ Silymarin (%w/w)	Size (nm) ^a	Pdl ^a	HC cycle ^b	ω (nm ³ /h)
F1 C-0.20				
SM-0.5	112.7 ± 0.51	0.208 ± 0.00	6 cycles	970.89
SM-0.75	115.0 ± 0.92	0.185 ± 0.025	5 cycles	2913.4

^a Data of freshly prepared nanoemulsion; reported as mean ± SD, n=3

^b HC Cycle, heating-cooling cycle, reported as the number of stable cycle(s)

ω : Ostwald ripening rate



C. Characterization of silymarin nanoemulsion gel

1. Entrapment efficiency (EE)

Ultracentrifugation method is commonly used for phase separation by gravity force in any suspension. Speed of centrifugation at 15,000 rpm for 1 hour was preliminarily used to separate SMNE gel but SMNE gel could not be separated with this condition. Therefore, ultracentrifugation speeds were varied at 40,000, 50,000, 60,000 and 65,000 rpm for fixed 1 hour duration at 25 °C. After ultracentrifugation at higher speeds, separated SMNE gels are shown in Figure 9. Regarding to density, the upper layer should be the mixture of internal phase (oil, surfactant and most of silymarin), which silymarin mostly dissolved in o/w interfacial layer and partly linked with some parts of gelling agent and water. Two separated phases were collected and analyzed by a validated UV-Vis spectrophotometric method (Section D). The results showed that % EE of 40,000, 50,000, 60,000 and 65,000 rpm were 89.78, 86.65, 83.14 and 80.28, respectively. The speed of 60,000 rpm was chosen due to clear separation obtained with an acceptable speed. SMNE gels were performed in triplicates and the EE were 83.91 ± 0.63 %.

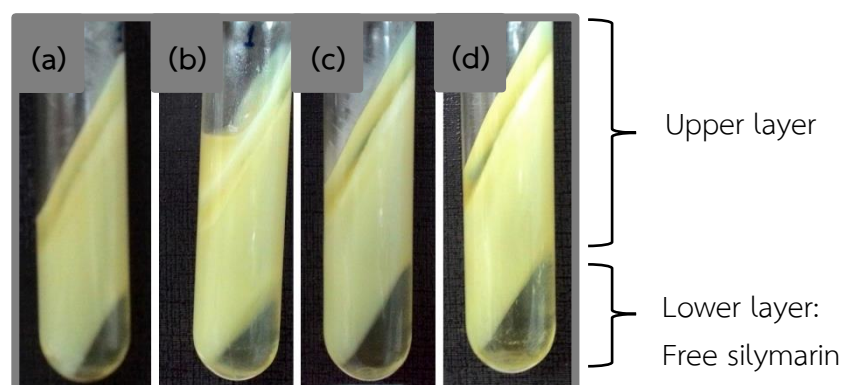


Figure 9 Silymarin nanoemulsion gels after ultracentrifugation at (a) 40,000 rpm, (b) 50,000 rpm, (c) 60,000 rpm and (d) 65,000 rpm for one hour at 25 °C

2. Drug content

Freshly prepared SMNE gels were extracted by methanol and analyzed by a validated HPLC method (Section D). The results showed that the mean of silymarin content was 0.527 ± 0.004 %w/w.

3. Chemical stability

Silymarin contents in SMNE gels were analyzed by a validated quantitative analysis HPLC method in Section D. The percentages of silymarin remaining in nanoemulsion gel were plotted versus storage time (Figure 10). Silymarin content decreased by time during stored in the accelerated condition (40 °C) for three months. As can be seen in Figure 10, % silymarin remaining of SMNE gel dramatically decreased to 42.47 ± 1.92 % after three-months of storage.

Silymarin was showed considerably stable in stability tests stressed by acidic hydrolysis (hydrochloric acid), neutral hydrolysis (70 °C), photo-degradation (sun light; 8 hours) or dry heat (105 °C) (Korany et al., 2013). However, it was partially degraded by oxidative degradation (hydrogen peroxide) and totally destroyed by alkaline hydrolysis (sodium hydroxide). This report indicated that silymarin could tolerate to heat both in aqueous solution and dry heat. Consequently, silymarin loaded nanostructured lipid carriers (NLC) (Lawanwadeekul, 2011) and also silybin loaded NLC (Jia et al., 2010) could be prepared by hot high pressure homogenization method which the actives were still stable after the process. Silymarin should be stable under the storage condition at 40 °C in this study. In conclusion, silymarin could be possibly degraded by oxidative hydrolysis but not with heat.

Chemical stability studies of silymarin microemulsions (Panapisal et al., 2012) at the same storage condition, % silymarin remaining of Tween[®] 20 microemulsions were less than that of Labrasol[®] microemulsions. Although, the total number of

oxyethelene groups in Tween[®] 20 is comparable to those of Labrasol[®] when considering as moles/g of microemulsion, the sorbitan ring of Tween[®] 20 may cause steric hindrance against flavonolignans of silymarin to form hydrogen bonds, which may keep silymarin inside the interface and prevent it from being oxidized. Meanwhile, flavonolignans of silymarin may prefer to localize in Labrasol[®] (or interface) resulting in superior stability from being oxidized than other formulations. For this reason, SMME gel consisting of Tween[®] 20 may also provide less drug protection when silymarin localized in surfactant layer and may slowly partition into the water phase and subject to oxidation and degradation.

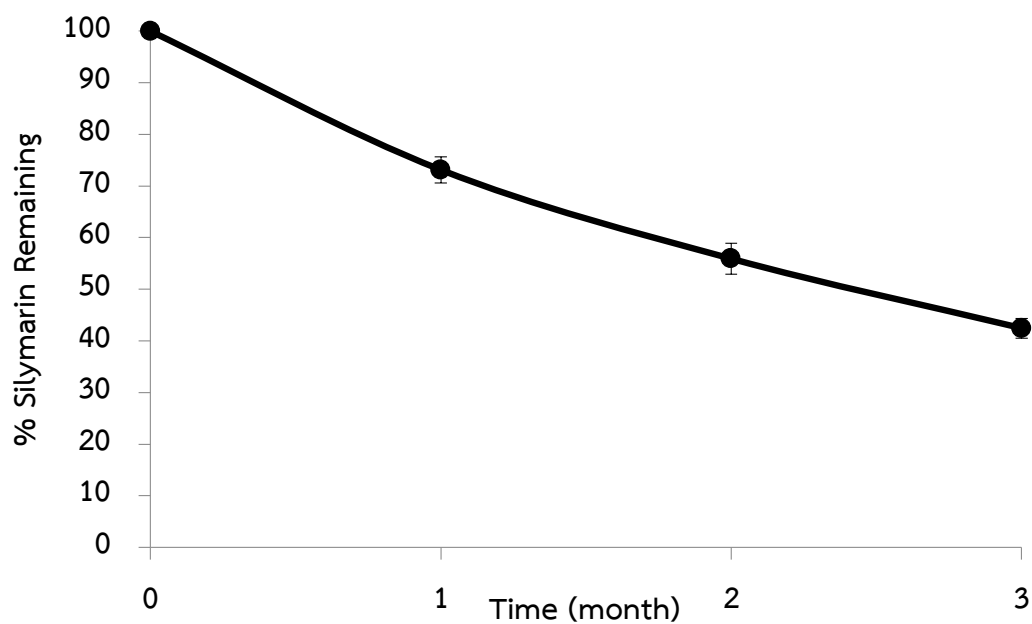


Figure 10 Chemical stabilities of silymarin nanoemulsion gel at 40 °C.

4. *In vitro* release study

In vitro releases of silymarin from nanoemulsion gel (SMNE gel), microemulsion (SMME) and solution were determined using modified Franz diffusion cell with cellulose membrane. 40 % ethanol in PBS was used as receptor solution to maintain sink conditions referred to the method of Panapisal (2012). All formulations were prepared with an equal amount of silymarin (0.5 %w/w). The released silymarin content was analyzed by UV-Vis spectrophotometric method validated in Section E. The plot between percentage cumulative release of silymarin versus time is shown in Figure 11. The results showed that silymarin solution rapidly released at the first hour and reached 94 % cumulative amount at 24 hours. Silymarin gradually released from both SMNE gel and SMME; however SMNE gel showed faster release rate than that of SMME. Nanoemulgel could be used as a sustained-release formulation when compared with nanoemulsions as shown in many reports of *in vitro* release of nanoemulsions and nanoemulgel (Baboota et al., 2007; Hussain et al., 2016; Shakeel, Ramadan and Ahmed, 2009). This may imply that silymarin nanoemulsion (without gel agent) should have even higher release rate than silymarin microemulsion. In this study, SMNE gel showed much higher viscosity of 142.20 cP whereas SMME showed 45.80 cP but SMNE gel revealed higher drug release. Besides viscosity, particle size could also influence the drug release from the system. Smaller particle size should release faster than larger one. SMNE gel and SMME showed comparable particle sizes of 112.7 nm and 114.2 nm, respectively. Therefore, neither viscosity or particle size may not significantly influence the drug release from the systems in the present study. These results showed support for our hypothesis that was less drug-system affinity should be anticipated with lower amount of surfactant used in nanoemulsion resulting in higher amount of silymarin released. The release studies of plaunoi extract loaded nanoemulsion and microemulsion showed consistency that release

rate of nanoemulsion was significantly higher than that of w/o microemulsion, o/w microemulsion and emulsion (Songkro et al., 2011).

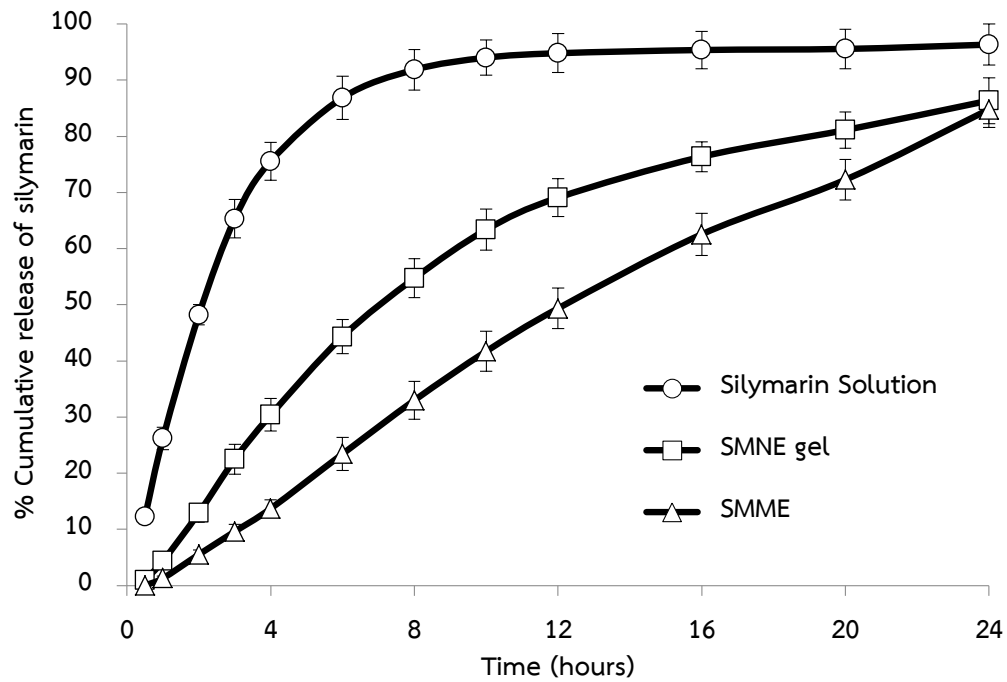


Figure 11 Release profiles of silymarin nanoemulsion gel (SMNE gel), silymarin microemulsion (SMME) and silymarin solution (mean \pm SD, n=3)

D. Quantitative analysis of silymarin by high performance liquid chromatographic (HPLC) method

The HPLC method was used to analyze silymarin content in the studies of drug content and chemical stability. The purpose of validation of an analytical procedure is to demonstrate that it is suitable for its intended analytical applications (ICH guidelines on topic Q2 (R1), 2005). In this study, the HPLC method of silymarin analysis (Panapisal et al., 2012) was validated. Because of silymarin extract composes of many flavonolignans, silybin A and B, which are the major components of silymarin, were used as reference peaks for silymarin quantitative analysis by HPLC method.

1. Specificity

The specificity of analytical method is the ability to differentiate and quantify silymarin in the presence of other compositions in the sample.

The chromatograms of methanol, which was used as dilution solvent, silybin (silybin A and B) standard solution, silymarin standard solution, blank nanoemulsion gel, silymarin nanoemulsion gel are shown in Figure 12. All chromatograms are shown under the same attenuation.

There was no interference from other compositions including other flavonolignans in silymarin, oil, surfactant and gelling agent in nanoemulsion and solvent to the reference peaks (i.e., silybin A and B). Therefore, this HPLC method was acceptable for specificity.

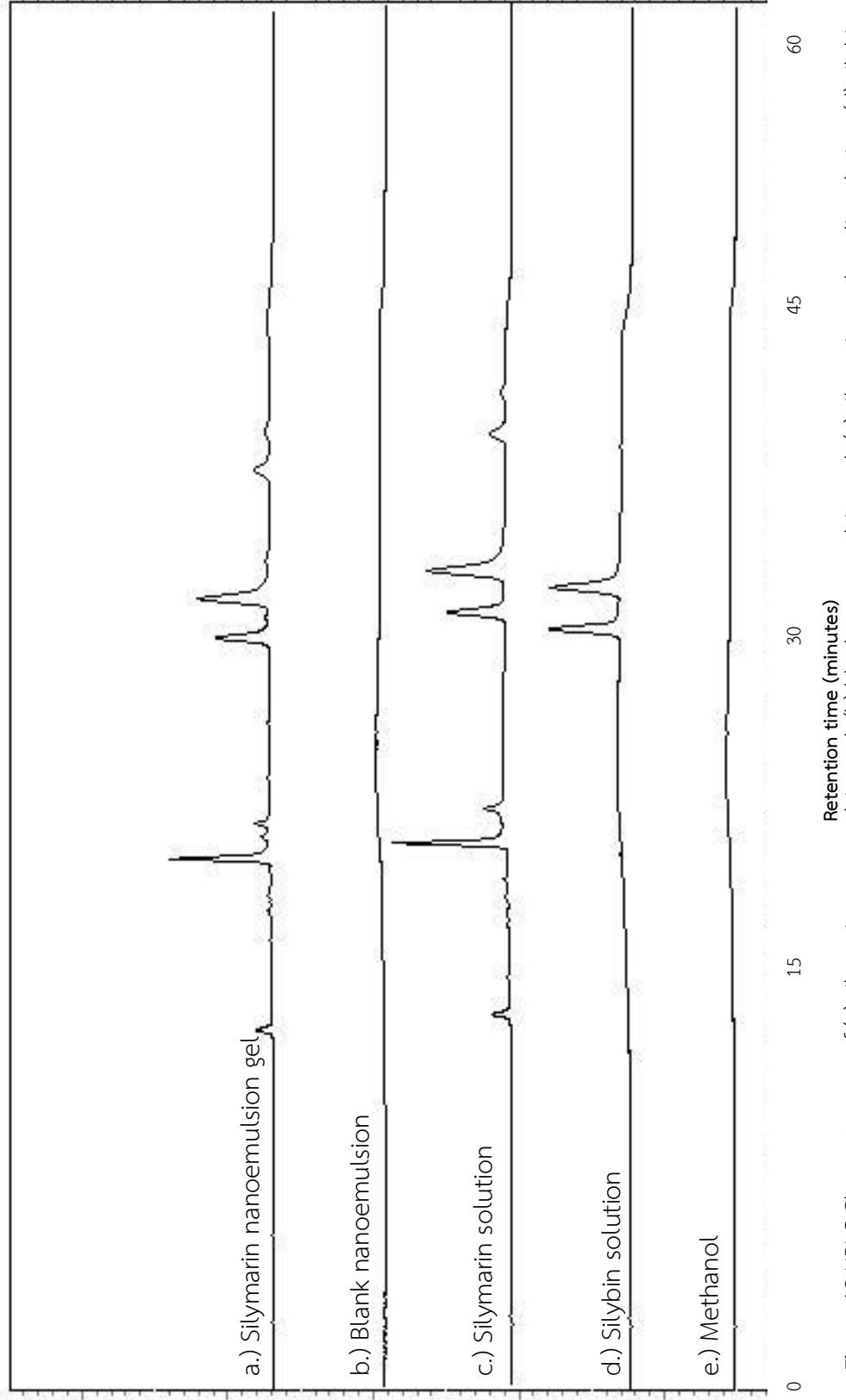


Figure 12 HPLC Chromatograms of (a) silymarin nanoemulsion gel, (b) blank nanoemulsion gel, (c) silymarin methanolic solution, (d) silybin and (e) methanol

2. Linearity

The linearity of an analytical method is its ability, within a given range, to obtain test results which are directly, or by a mathematical transformation, proportional to the concentration of analyte in the sample.

The representative calibration curve data of silybin reference solutions are shown in Table 8. The plot between silybin concentrations and the sum of peak area (Figure 13) illustrated the linear correlation in the concentration range of 2-20 $\mu\text{g/mL}$. The coefficient of determination (R^2) was 0.9996. The results indicated that the HPLC method was suitable for silymarin quantitative analysis by this HPLC method.

The representative calibration curve data of silymarin standard solutions are shown in Table 9. The plot between silymarin concentration and the sum peak area of silybin A and silybin B (Figure 14) illustrated the linear correlation in the concentration range of 6-60 $\mu\text{g/mL}$. The coefficient of determination (R^2) was 0.9995. The sum of silybin A and silybin B contents in silymarin was found about 30%, which was the approximate amount of silybins in the standardized silymarin extract. The results indicated that the HPLC method was acceptable for silymarin quantitative analysis in the studied range.

Table 8 The data of silybin for calibration curve by HPLC method

Concentration of silybin ($\mu\text{g/mL}$)	Sum peak area of silybin A and B			Mean	SD	%CV
	SET 1	SET 2	SET 3			
	2	44213	44222			
4	99378	98506	97623	98502.33	877.51	0.89
8	183920	183192	184848	183986.67	830.01	0.45
12	276010	280921	282491	279807.33	3380.98	1.21
16	377550	376074	376256	376626.67	804.79	0.21
20	471029	467469	467096	468531.33	2171.07	0.46

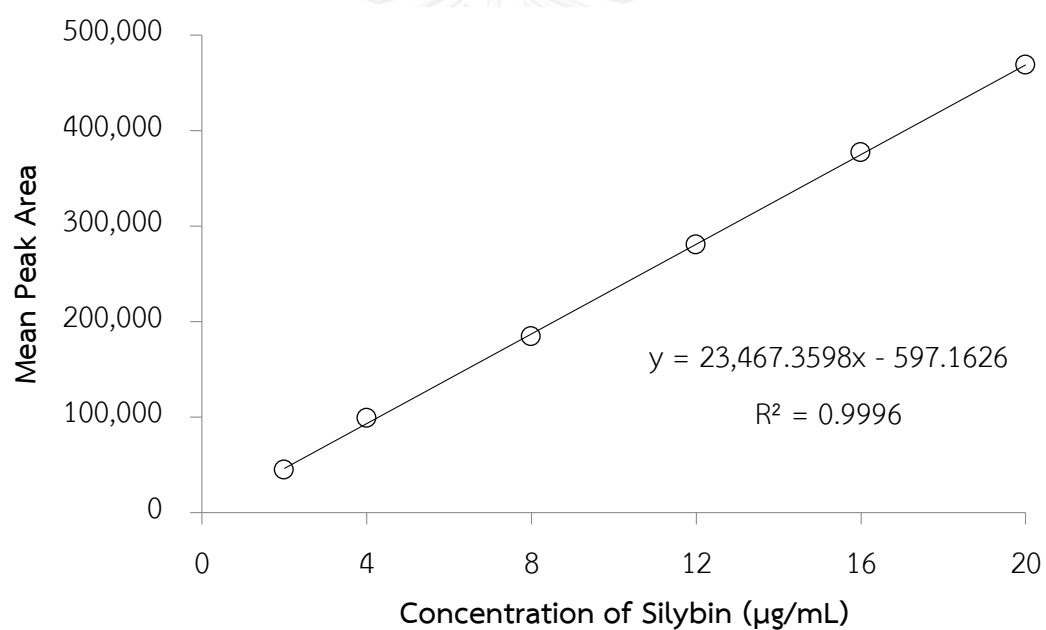
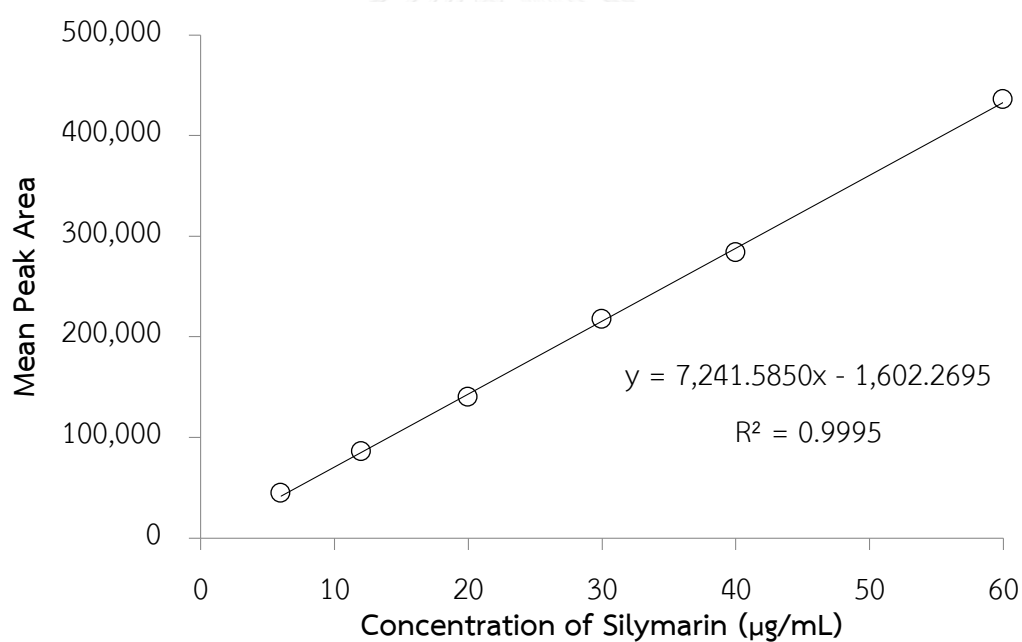
**Figure 13** Calibration curve of silybin by HPLC method

Table 9 The data of silymarin for calibration curve by HPLC method

Concentration of silymarin ($\mu\text{g/mL}$)	Sum peak area of silybin A and B			Mean	SD	%CV
	SET 1	SET 2	SET 3			
6	42058	44356	46480	44298.00	2211.57	4.99
12	81928	86093	89887	85969.33	3980.94	4.63
20	134001	141366	145116	140161.00	5654.63	4.03
30	211474	215395	224929	217266.00	6919.88	3.19
40	273363	283606	293638	283535.67	10137.68	3.58
60	416725	437510	452993	435742.67	18198.48	4.18

**Figure 14** Calibration curve of silymarin by HPLC method

3. Accuracy

The accuracy of an analytical method expresses the closeness of agreement between the value which is accepted either as a conventional true value or an accepted reference value and the value found. The accuracy was assessed using three concentration levels covering the specified range.

The percentages of analytical recovery were in the range of 99.20-108.11 % (Table 10), indicated that this HPLC method could be used for silymarin analysis in the range with high accuracy.

Table 10 The percentages of analytical recovery of silymarin by HPLC method

Concentration of silymarin ($\mu\text{g/mL}$)	%Analytical recovery					Mean	SD	%CV
	SET 1	SET 2	SET 3	SET 4	SET 5			
10	101.17	105.08	103.74	103.05	108.06	104.22	2.57	2.46
25	99.77	101.97	99.54	104.08	107.13	102.50	3.18	3.10
45	99.20	106.48	99.51	102.03	108.11	103.07	4.06	3.93

4. Precision

The precision of an analytical method expresses the closeness of agreement between a series of measurements obtained from multiple sampling of the same homogenous sample under the prescribed conditions. The precision assesses using three concentration levels covering the specified range.

The precision were determined both for repeatability and intermediate runs, which were expressed as the coefficient of variation (% CV) in Tables 11 and 12. The coefficient of variation values of repeatability and intermediate runs were in the range of 2.46-3.93 % and 1.79-3.11 %, respectively. This indicated that this HPLC method was precise for silymarin analysis in the studied range.

4.1 Repeatability (within run precision)

Table 11 Data of repeatability of silymarin by HPLC method

Concentration of silymarin ($\mu\text{g/mL}$)	Estimated concentration ($\mu\text{g/mL}$)					Mean	SD	%CV
	SET 1	SET 2	SET 3	SET 4	SET 5			
10	10.12	10.51	10.37	10.31	10.81	10.42	0.26	2.46
25	24.94	25.49	24.88	26.02	26.78	25.62	0.80	3.10
45	44.64	47.92	44.78	45.92	48.65	46.38	1.83	3.93

4.2 Intermediate precision (between run precision)

Table 12 Data of intermediate precision of silymarin by HPLC method

Concentration of silymarin ($\mu\text{g/mL}$)	Estimated concentration ($\mu\text{g/mL}$)					Mean	SD	%CV
	SET 1	SET 2	SET 3	SET 4	SET 5			
10	10.12	10.56	10.22	10.22	9.68	10.16	0.32	3.11
25	24.94	25.83	25.18	25.27	24.38	25.12	0.53	2.11
45	44.64	46.22	45.16	46.62	46.10	45.75	0.82	1.79

5. Limit of detection (LOD)

The lowest concentration of silymarin that this HPLC method could be detected was $1.56 \mu\text{g/mL}$. In other words, the analytical method may identify the peaks of silybin A and silybin B, but the results could not express as accurate amount when repeating the experiment.

6. Limit of quantitation (LOQ)

The lowest concentration of silymarin that this HPLC method could be detected correctly for quantitative analysis was $4.74 \mu\text{g/mL}$.

E. Quantitative analysis of silymarin by UV-Vis spectrophotometric method

The UV-Vis spectrophotometric method was used to analyze silymarin content for entrapment efficiency and release studies instead of time-consuming HPLC method. The method was validated as follows:

1. Specificity

1.1 Entrapment efficiency

The wavelengths scan between 200 – 400 nm of silymarin in methanol (25 µg/mL) showed the maximum absorbance at 288 nm. Blank nanoemulsion gel (F1) showed no absorbance at 288 nm. Blank nanoemulsion spiked silymarin (25 µg/mL) and SMNE gel (25 µg/mL) in methanol solution showed no interference by excipients and had the same maximum wavelength absorbance at 288 nm and the absorbance unit as silymarin in methanolic solution (25 µg/mL).

1.2 *in vitro* release study

The wavelengths scan between 200 – 400 nm of silymarin in 40 % ethanol – PBS (10 µg/mL) showed the maximum absorbance at 329 nm. Blank nanoemulsion gel (F1) showed no absorbance at 329 nm. Blank nanoemulsion spiked silymarin (10 µg/mL) and SMNE gel (10 µg/mL) in 40 % ethanol – PBS showed no interference by excipients and had the same maximum wavelength absorbance at 329 nm and the absorbance unit as silymarin in 40 % ethanol – PBS (10 µg/mL).

At the same concentration level of silymarin in methanol and in 40 % ethanol – PBS showed the same absorbance value, which the validation (linearity, accuracy and precision) of silymarin in 40 % ethanol – PBS would not be necessary.

2. Linearity

The calibration curve data of silymarin in methanolic solutions in the concentration range of 4-20 $\mu\text{g/mL}$ are represented in Table 13 and the graph plot of silymarin concentrations versus absorbance at 288 nm is shown in Figure 15. The coefficient of determination (R^2) on the linear correlation was 0.99999. The results indicated that the UV-Vis spectroscopic method was acceptable for quantitative analysis of silymarin in the study range.

Table 13 The calibration curve data of silymarin in methanolic solution by UV-Vis spectrophotometric method

Concentration of silymarin ($\mu\text{g/mL}$)	Absorbance at 288 nm			Mean	SD	% CV
	SET 1	SET 2	SET 3			
4	0.1774	0.1836	0.1840	0.1817	0.0037	2.0369
6	0.2636	0.2677	0.2650	0.2654	0.0021	0.7852
8	0.3466	0.3514	0.3472	0.3484	0.0026	0.7507
10	0.4296	0.4326	0.4330	0.4317	0.0019	0.4304
15	0.6343	0.6415	0.6391	0.6383	0.0037	0.5743
20	0.8499	0.8509	0.8472	0.8493	0.0019	0.2254

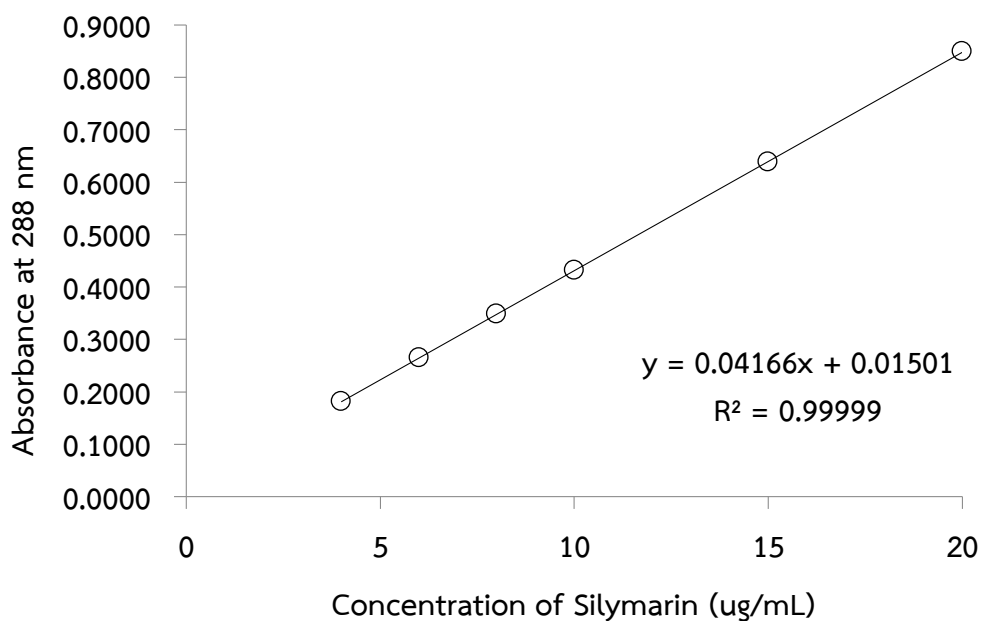


Figure 15 Calibration curve of silymarin in methanolic solution by UV-Vis spectrophotometric method

3. Accuracy

The percentages of analytical recovery were in the range of 98.94-103.66 % (Table 14), which indicated that this UV-Vis spectrophotometric method could be used for silymarin analysis in the range with high accuracy.

Table 14 The percentage of analytical recovery of silymarin in methanolic solution by UV-Vis spectrophotometric method

Concentration of silymarin ($\mu\text{g/mL}$)	% Analytical recovery					Mean	SD	%CV
	SET 1	SET 2	SET 3	SET 4	SET 5			
5	100.62	103.66	102.12	101.48	98.94	101.37	1.75	1.73
9	102.16	102.22	102.09	100.16	100.06	101.34	1.12	1.11
18	101.85	102.09	101.11	99.35	99.66	100.81	1.25	1.24

4. Precision

The precision was determined both for repeatability and intermediate runs, which were expressed as the coefficient of variation (% CV) in Tables 15 and 16. The coefficient of variation values of repeatability and intermediate runs were in the range of 1.11-1.73 % and 0.70-0.89 %, respectively. The results indicated that this UV-Vis spectrophotometric method was precise for silymarin analysis in the range.

Table 15 Data of repeatability of silymarin by UV-Vis spectrophotometric method

Concentration of silymarin ($\mu\text{g/mL}$)	Estimated concentration ($\mu\text{g/mL}$)					Mean	SD	%CV
	SET 1	SET 2	SET 3	SET 4	SET 5			
5	5.03	5.18	5.11	5.07	4.95	5.07	0.09	1.73
9	9.19	9.20	9.19	9.01	9.01	9.12	0.10	1.11
18	18.33	18.38	18.20	17.88	17.94	18.15	0.22	1.24

Table 16 Data of intermediate precision of silymarin by UV-Vis spectrophotometric method

Concentration of silymarin ($\mu\text{g/mL}$)	Estimated concentration ($\mu\text{g/mL}$)					Mean	SD	%CV
	SET 1	SET 2	SET 3	SET 4	SET 5			
5	5.07	5.00	5.02	5.11	5.04	5.05	0.04	0.89
9	9.01	9.07	8.98	9.09	8.93	9.02	0.06	0.70
18	17.88	18.02	17.86	17.99	17.68	17.89	0.14	0.76

CHAPTER 5

CONCLUSIONS

In this present study, nanoemulsions were chosen to deliver silymarin to the skin. Surfactant and cosurfactant in terms of concentration and smix ratio had an influence on the physical properties and physical stability of prepared nanoemulsions. Smaller particle sizes were obtained when using high smix concentration whereas larger particle sizes were obtained when increasing proportion of Transcutol[®]. Another undesired results when using Transcutol[®] were that the formulations containing Transcutol[®] showed less stable than the formulation without Transcutol[®] in accelerated conditions. Blank nanoemulsion without Transcutol[®] (F1) was chosen to incorporate silymarin. 0.2 %w/w Carbopol[®] 940 was used to improve physical stability of blank nanoemulsion. The addition of gelling agent did not alter its particle size and made it pass the heating-cooling test. Particle size of silymarin nanoemulsion gel was in the nano-size range of 112.7 ± 0.51 nm with considerably high entrapment efficiency of 83.91 ± 0.63 %. Silymarin nanoemulsion gel loaded with 0.5 %w/w silymarin presented physically stable after six heating-cooling cycles but was chemically instable during storage at 40 °C for three months which silymarin gradually degraded. Silymarin nanoemulsion gel showed higher amount of silymarin released than silymarin microemulsion regarding to expected lower drug-system affinity from less surfactant used. For further studies, skin permeation of silymarin nanoemulsion gel should be compared with silymarin microemulsion, as well as skin irritation and its efficacy.

REFERENCES

- Altaei, T. (2012). "The treatment of melasma by silymarin cream." BioMed Central Dermatology 12(1): 18.
- Alvarado, H. L., G. Abrego, E. B. Souto, M. L. Garduño-Ramirez, B. Clares, M. L. García and A. C. Calpena (2015). "Nanoemulsions for dermal controlled release of oleanolic and ursolic acids: *In vitro*, *ex vivo* and *in vivo* characterization." Colloids and Surfaces B: Biointerfaces 130(0): 40-47.
- Anthony, K. P. and M. A. Saleh (2013). "Free radical scavenging and antioxidant activities of silymarin components." Antioxidants 2(4): 398-407.
- Ashkani-Esfahani, S., Y. Emami, E. Esmaeilzadeh, F. Bagheri, M. R. Namazi, M. Keshtkar, M. Khoshneviszadeh and A. Noorafshan (2013). "Silymarin enhanced fibroblast proliferation and tissue regeneration in full thickness skin wounds in rat models; a stereological study." Journal of the Saudi Society of Dermatology and Dermatologic Surgery 17(1): 7-12.
- Baboota, S., F. Shakeel, A. Ahuja, J. Ali and S. Shafiq (2007). Design, development and evaluation of novel nanoemulsion formulations for transdermal potential of celecoxib. Acta Pharmaceutica. 57: 315.
- Choo, S. J., I. J. Ryoo, Y. H. Kim, G. H. Xu, W. G. Kim, K. H. Kim, S. J. Moon, E. D. Son, K. Bae and I. D. Yoo (2009). "Silymarin inhibits melanin synthesis in melanocyte cells." Journal of Pharmacy and Pharmacology 61(5): 663-667.
- Clares, B., A. C. Calpena, A. Parra, G. Abrego, H. Alvarado, J. F. Fangueiro and E. B. Souto (2014). "Nanoemulsions (NEs), liposomes (LPs) and solid lipid nanoparticles (SLNs) for retinyl palmitate: effect on skin permeation." International Journal of Pharmaceutics 473(1-2): 591-598.

- Couteau, C., M. Pommier, E. Papis and L. J. Coiffard (2007). "Study of the efficacy of 18 sun filters authorized in European Union tested in vitro." Pharmazie 62(6): 449-452.
- Couteau, C., C. Cheignon, E. Papis and L. J. M. Coiffard (2011). "Silymarin, a molecule of interest for topical photoprotection." Natural Product Research 26(23): 2211-2214.
- Davis-Searles, P. R., Y. Nakanishi, N. C. Kim, T. N. Graf, N. H. Oberlies, M. C. Wani, M. E. Wall, R. Agarwal and D. J. Kroll (2005). "Milk thistle and prostate cancer: differential effects of pure flavonolignans from *Silybum marianum* on antiproliferative end points in human prostate carcinoma cells." Cancer Research 65(10): 4448-4457.
- Dixit, N., K. Kohli and S. Baboota (2008). "Nanoemulsion system for the transdermal delivery of a poorly soluble cardiovascular drug." PDA Journal of Pharmaceutical Science and Technology 62(1): 46-55.
- Elfar, N. N. and G. M. El-Maghraby (2015). "Efficacy of intradermal injection of tranexamic acid, topical silymarin and glycolic acid peeling in treatment of melasma: a comparative study." Journal of Clinical and Experimental Dermatology Research 06(03).
- Faezizadeh, Z., A. Gharib and M. Godarzee (2015). "*In-vitro* and *in-vivo* evaluation of silymarin nanoliposomes against isolated methicillin-resistant *Staphylococcus aureus*." Iranian Journal of Pharmaceutical Research 14(2): 627-633.
- Gazak, R., A. Svobodova, J. Psotova, P. Sedmera, V. Prikrylova, D. Walterova and V. Kren (2004). "Oxidised derivatives of silybin and their antiradical and antioxidant activity." Bioorganic and Medical Chemistry 12(21): 5677-5687.
- Gutiérrez, J. M., C. González, A. Maestro, I. Solè, C. M. Pey and J. Nolla (2008). "Nano-emulsions: New applications and optimization of their preparation." Current Opinion in Colloid and Interface Science 13(4): 245-251.

- Han, M. H., W. K. Yoon, H. Lee, S. B. Han, K. Lee, S. K. Park, K. H. Yang, H. M. Kim and J. S. Kang (2007). "Topical application of silymarin reduces chemical-induced irritant contact dermatitis in BALB/c mice." International Immunopharmacology 7(13): 1651-1658.
- Hung, C. F., Y. K. Lin, L. W. Zhang, C. H. Chang and J. Y. Fang (2010). "Topical delivery of silymarin constituents via the skin route." Acta Pharmacologica Sinica 31(1): 118-126.
- Hussain, A., A. Samad, S. K. Singh, M. N. Ahsan, M. W. Haque, A. Faruk and F. J. Ahmed (2016). "Nanoemulsion gel-based topical delivery of an antifungal drug: *in vitro* activity and in vivo evaluation." Drug Delivery 23(2): 652-667.
- Jia, L., D. Zhang, Z. Li, C. Duan, Y. Wang, F. Feng, F. Wang, Y. Liu and Q. Zhang (2010). "Nanostructured lipid carriers for parenteral delivery of silybin: Biodistribution and pharmacokinetic studies." Colloids and Surfaces B: Biointerfaces 80(2): 213-218.
- Junyaprasert, V. B., V. Teeranachaideekul, E. B. Souto, P. Boonme and R. H. Muller (2009). "Q10-loaded NLC versus nanoemulsions: stability, rheology and *in vitro* skin permeation." International Journal of Pharmaceutics 377(1-2): 207-214.
- Katiyar, S. K., N. J. Korman, H. Mukhtar and R. Agarwal (1997). "Protective effects of silymarin against photocarcinogenesis in a mouse skin model." Journal of the National Cancer Institute 89(8): 556-566.
- Katiyar, S. K., A. M. Roy and M. S. Baliga (2005). "Silymarin induces apoptosis primarily through a p53-dependent pathway involving Bcl-2/Bax, cytochrome c release, and caspase activation." Molecular Cancer Therapeutics 4(2): 207-216.

- Koksal, E., I. Gulcin, S. Beyza, O. Sarikaya and E. Bursal (2009). "*In vitro* antioxidant activity of silymarin." Journal of Enzyme Inhibition and Medicinal Chemistry 24(2): 395-405.
- Korany, M. A., R. S. Haggag, M. A. A. Ragab and O. A. Elmallah (2013). "A validated stability-indicating HPLC method for simultaneous determination of Silymarin and Curcumin in various dosage forms." Arabian Journal of Chemistry.
- Křen, V. and D. Walterová (2005). "Silybin and silymarin - new effects and applications." Biomedical papers 149(1): 29-41.
- Kumar, D., M. Aqil, M. Rizwan, Y. Sultana and M. Ali (2009). "Investigation of a nanoemulsion as vehicle for transdermal delivery of amlodipine." Pharmazie 64(2): 80-85.
- Lawanwadeekul, S. (2011). Formulation of silymarin-loaded nanostructured lipid carriers for dermal delivery. Master of Science in Pharmacy Program in Pharmaceutics, Department of Pharmaceutics and Industrial Pharmacy, Faculty of Pharmaceutical Sciences, Chulalongkorn University.
- Liu, L., X. Pang, W. Zhang and S. Wang (2007). "Formulation design and *in vitro* evaluation of silymarin-loaded self-microemulsifying drug delivery systems." Asian Journal of Pharmaceutical Sciences 2(4): 150-160.
- McClements, D. J. (1994). "Ultrasonic determination of depletion flocculation in oil-in-water emulsions containing a non-ionic surfactant." Colloids and Surfaces A: Physicochemical and Engineering Aspects 90(1): 25-35.
- Meeran, S. M., S. Katiyar, C. A. Elmets and S. K. Katiyar (2006). "Silymarin inhibits UV radiation-induced immunosuppression through augmentation of interleukin-12 in mice." Molecular Cancer Therapeutics 5(7): 1660-1668.

- Mura, S., M. Manconi, D. Valenti, C. Sinico, A. O. Vila and A. M. Fadda (2011). "Transcutol containing vesicles for topical delivery of minoxidil." Journal of Drug Targeting 19(3): 189-196.
- Panapisal, V., S. Charoensri and A. Tantituvanont (2012). "Formulation of microemulsion systems for dermal delivery of silymarin." AAPS PharmSciTech 13(2): 389-399.
- Rasul, A., N. Akhtar, B. A. Khan, T. Mahmood, S. u. Zaman, A. Ali, H. M. S. Khan and R. Parveen (2011). "Assessment of anti erythmic and skin whitening effects of milk thistle extract." African Journal of Pharmacy and Pharmacology 5(20).
- Rasul, A. and N. Akhtar (2012). "Anti-aging potential of a cream containing milk thistle extract: Formulation and *in vivo* evaluation." African Journal of Biotechnology 11(6).
- Rocha-Filho, P., M. Maruno, B. Oliveira, D. Bernardi, V. Gumiero and T. Pereira (2014). "Nanoemulsions as a vehicle for drug and cosmetics." Nanoscience and Technology 1(1).
- Shakeel, F., W. Ramadan and M. A. Ahmed (2009). "Investigation of true nanoemulsions for transdermal potential of indomethacin: characterization, rheological characteristics, and *ex vivo* skin permeation studies." Journal of Drug Targeting 17(6): 435-441.
- Sharma, S., J. K. Sahni, J. Ali and S. Baboota (2015). "Effect of high-pressure homogenization on formulation of TPGS loaded nanoemulsion of rutin - pharmacodynamic and antioxidant studies." Drug Delivery 22(4): 541-551.
- Songkro, S., W. Pichayakorn, S. Sungkarak and J. Wungsintaweekul (2011). "Investigation of plaunoi-loaded micro/nanoemulsions for the treatment of dermatitis: formulation, évaluation and skin irritation studies." Journal of Drug Delivery Science and Technology 21(5): 401-410.

- Spada, G., E. Gavini, M. Cossu, G. Rassa, A. Carta and P. Giunchedi (2013). "Evaluation of the effect of hydroxypropyl-beta-cyclodextrin on topical administration of milk thistle extract." Carbohydrate Polymers 92(1): 40-47.
- Sullivan Jr, D. W., S. C. Gad and M. Julien (2014). "A review of the nonclinical safety of Transcutol[®], a highly purified form of diethylene glycol monoethyl ether (DEGEE) used as a pharmaceutical excipient." Food and Chemical Toxicology 72: 40-50.
- Svobodova, A., D. Walterova and J. Psotova (2006). "Influence of silymarin and its flavonolignans on H₂O₂-induced oxidative stress in human keratinocytes and mouse fibroblasts." Burns 32(8): 973-979.
- Svobodova, A., A. Zdarilova, D. Walterova and J. Vostalova (2007). "Flavonolignans from *Silybum marianum* moderate UVA-induced oxidative damage to HaCaT keratinocytes." Journal of Dermatological Science 48(3): 213-224.
- Tadros, T., P. Izquierdo, J. Esquena and C. Solans (2004). "Formation and stability of nano-emulsions." Advances in Colloid and Interface Science 108–109: 303-318.
- Talegaonkar, S. and L. M. Negi (2015). Nanoemulsion in Drug Targeting. Targeted Drug Delivery : Concepts and Design. V. P. Devarajan and S. Jain. Cham, Springer International Publishing: 433-459.
- Tang, S. Y., P. Shridharan and M. Sivakumar (2013). "Impact of process parameters in the generation of novel aspirin nanoemulsions – Comparative studies between ultrasound cavitation and microfluidizer." Ultrasonics Sonochemistry 20(1): 485-497.
- Teeranachaideekul, V., E. B. Souto, V. B. Junyaprasert and R. H. Muller (2007). "Cetyl palmitate-based NLC for topical delivery of Coenzyme Q₁₀ - development, physicochemical characterization and in vitro release studies." European Journal of Pharmaceutics and Biopharmaceutics 67(1): 141-148.

- Theodosiou, E., K. Purchartová, H. Stamatis, F. Kolisis and V. Křen (2014). "Bioavailability of silymarin flavonolignans: drug formulations and biotransformation." Phytochemistry Reviews 13(1): 1-18.
- Uluata, S., E. A. Decker and D. J. McClements (2016). "Optimization of nanoemulsion fabrication using microfluidization: role of surfactant concentration on formation and stability." Food Biophysics 11(1): 52-59.
- Wang, X., Y. Jiang, Y. W. Wang, M. T. Huang, C. T. Ho and Q. Huang (2008). "Enhancing anti-inflammation activity of curcumin through O/W nanoemulsions." Food Chemistry 108(2): 419-424.
- Wollenweber, C., A. V. Makievski, R. Miller and R. Daniels (2000). "Adsorption of hydroxypropyl methylcellulose at the liquid/liquid interface and the effect on emulsion stability." Colloids and Surfaces A: Physicochemical and Engineering Aspects 172(1-3): 91-101.
- Woo, J. S., T. S. Kim, J. H. Park and S. C. Chi (2007). "Formulation and biopharmaceutical evaluation of silymarin using SMEDDS." Archives of Pharmacal Research 30(1): 82-89.
- Wooster, T. J., M. Golding and P. Sanguansri (2008). "Impact of oil type on nanoemulsion formation and ostwald ripening stability." Langmuir 24(22): 12758-12765.
- Yuan, Y., Y. Gao, J. Zhao and L. Mao (2008). "Characterization and stability evaluation of β -carotene nanoemulsions prepared by high pressure homogenization under various emulsifying conditions." Food Research International 41(1): 61-68.



APPENDICES

จุฬาลงกรณ์มหาวิทยาลัย
CHULALONGKORN UNIVERSITY

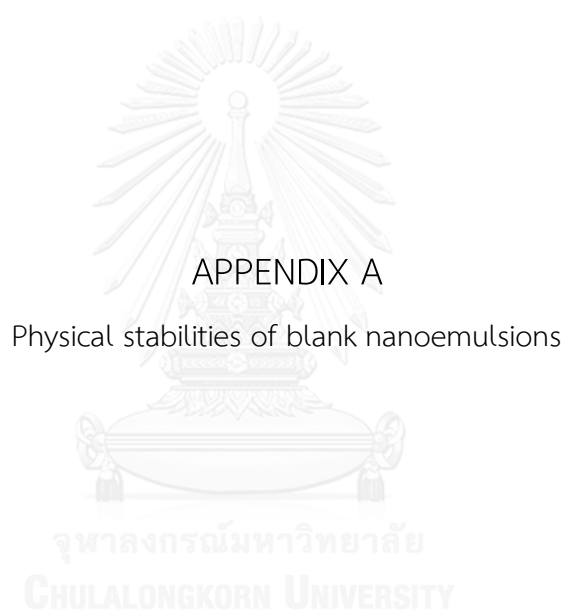


Table A-1 Physical stabilities of nanoemulsion F1

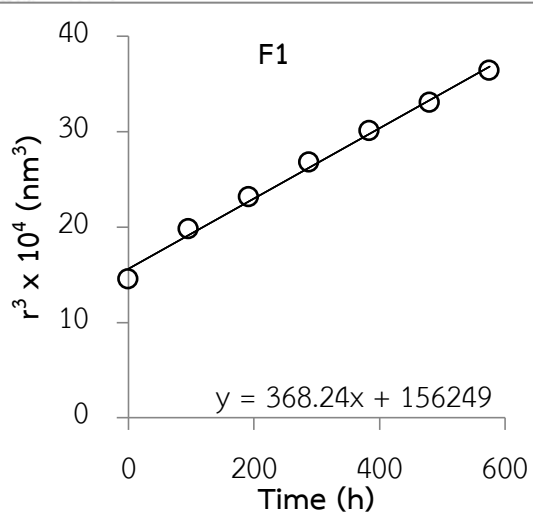
Heating-Cooling cycles

Cycle	At room temperature		At heating-cooling cycle	
	Size (d.nm)	Pdl	Size (d.nm)	Pdl
0	105.1 ± 0.17	0.192 ± 0.02	105.0 ± 0.17	0.192 ± 0.02
1	116.5 ± 0.75	0.128 ± 0.01	149.4 ± 0.54	0.081 ± 0.01
2	122.8 ± 0.38	0.130 ± 0.01	178.4 ± 1.45	0.061 ± 0.01
3	128.9 ± 1.25	0.109 ± 0.01	201.3 ± 0.99	0.056 ± 0.02
4	133.9 ± 0.68	0.102 ± 0.01	219.0 ± 1.20	0.058 ± 0.02
5	138.3 ± 0.92	0.098 ± 0.01	240.8 ± 2.11	0.090 ± 0.01
6	142.8 ± 0.91	0.088 ± 0.02	272.4 ± 5.83	0.118 ± 0.02

d.nm: diameter nanometer, Pdl: polydispersity index

Ostwald ripening rate at room temperature

Time (h)	Size (r.nm)	r^3 (nm ³)
0	52.6	145117.0
96	58.3	197813.9
192	61.4	231226.6
288	64.4	267575.5
384	67.0	300386.1
480	69.1	330340.6
576	71.4	363658.0
ω (nm ³ /h)	368.24	



The graph plots the cube of the radius, r^3 , in units of 10^4 nm^3 , against time in hours for nanoemulsion F1. The data points are approximately: (0, 14.5), (96, 19.8), (192, 23.1), (288, 26.8), (384, 30.0), (480, 33.0), (576, 36.4). A linear regression line is drawn through these points with the equation $y = 368.24x + 156249$.

r.nm: radius nanometer

ω : Ostwald ripening rate

Table A-2 Physical stabilities of nanoemulsion F2

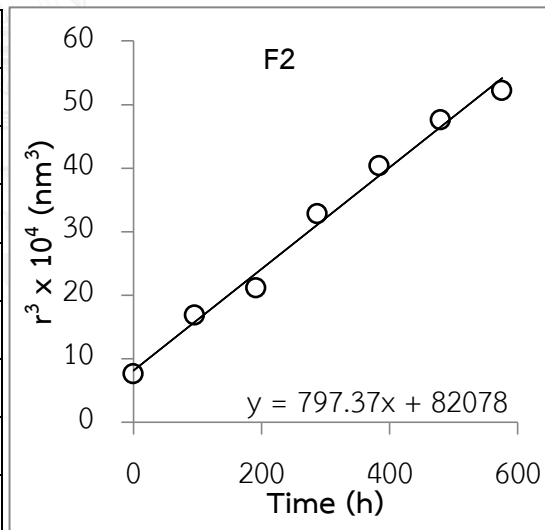
Heating-Cooling cycles

Cycle	At room temperature		At heating-cooling cycle	
	Size (d.nm)	Pdl	Size (d.nm)	Pdl
0	84.6 ± 0.22	0.211 ± 0.01	84.6 ± 0.22	0.211 ± 0.01
1	110.5 ± 1.53	0.111 ± 0.01	183.8 ± 2.68	0.052 ± 0.02
2	119.0 ± 4.26	0.086 ± 0.02	216.5 ± 7.05	0.047 ± 0.02
3	137.9 ± 1.24	0.072 ± 0.02	creaming	creaming
4	147.7 ± 0.47	0.066 ± 0.01	-	-
5	156.1 ± 0.69	0.078 ± 0.02	-	-
6	161.0 ± 1.26	0.049 ± 0.01	-	-

d.nm: diameter nanometer, Pdl: polydispersity index

Ostwald ripening rate at room temperature

Time (h)	Size (r.nm)	r^3 (nm ³)
0	42.3	75652.1
96	55.2	168503.0
192	59.5	210528.1
288	69.0	327795.4
384	73.9	402764.8
480	78.0	475364.7
576	80.5	521446.3
ω (nm ³ /h)	797.37	



r.nm: radius nanometer

ω : Ostwald ripening rate

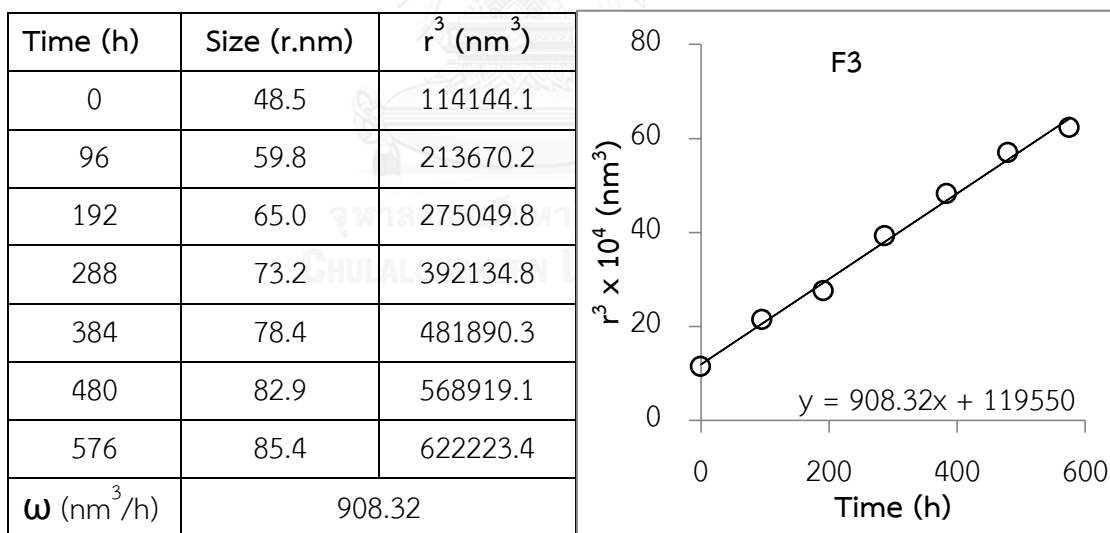
Table A-3 Physical stabilities of nanoemulsion F3

Heating-Cooling cycles of F3

Cycle	At room temperature		At heating-cooling cycle	
	Size (d.nm)	PdI	Size (d.nm)	PdI
0	97.0 ± 0.10	0.220 ± 0.01	97.0 ± 0.10	0.220 ± 0.01
1	119.6 ± 1.62	0.116 ± 0.01	201.9 ± 2.87	0.069 ± 0.02
2	130.0 ± 3.42	0.099 ± 0.02	249.5 ± 8.16	0.128 ± 0.03
3	146.4 ± 1.09	0.086 ± 0.02	creaming	creaming
4	156.8 ± 0.89	0.069 ± 0.02	-	-
5	165.7 ± 0.92	0.062 ± 0.02	-	-
6	170.7 ± 1.11	0.055 ± 0.02	-	-

d.nm: diameter nanometer

Ostwald ripening rate at room temperature



r.nm: radius nanometer

 ω : Ostwald ripening rate

Table A-4 Physical stabilities of nanoemulsion F4

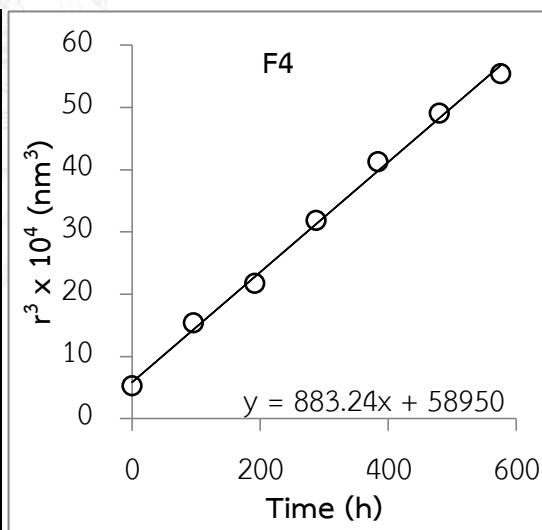
Heating-Cooling cycles

Cycle	At room temperature		At heating-cooling cycle	
	Size (d.nm)	Pdl	Size (d.nm)	Pdl
0	74.7 ± 0.18	0.201 ± 0.01	74.7 ± 0.18	0.201 ± 0.01
1	106.9 ± 1.47	0.097 ± 0.01	181.1 ± 2.49	0.054 ± 0.02
2	120.0 ± 3.44	0.078 ± 0.01	207.4 ± 6.20	0.054 ± 0.02
3	136.4 ± 1.03	0.061 ± 0.02	248.7 ± 1.83	0.083 ± 0.01
4	148.8 ± 0.67	0.059 ± 0.02	creaming	creaming
5	157.7 ± 0.86	0.081 ± 0.01	-	-
6	164.2 ± 1.57	0.048 ± 0.02	-	-

d.nm: diameter nanometer

Ostwald ripening rate at room temperature

Time (h)	Size (r.nm)	r^3 (nm ³)
0	37.3	52014.2
96	53.5	152748.6
192	60.0	216000.0
288	68.2	317291.3
384	74.4	412013.5
480	78.8	489928.2
576	82.1	553276.5
ω (nm ³ /h)	883.24	



r.nm: radius nanometer

 ω : Ostwald ripening rate

Table A-5 Physical stabilities of nanoemulsion F5

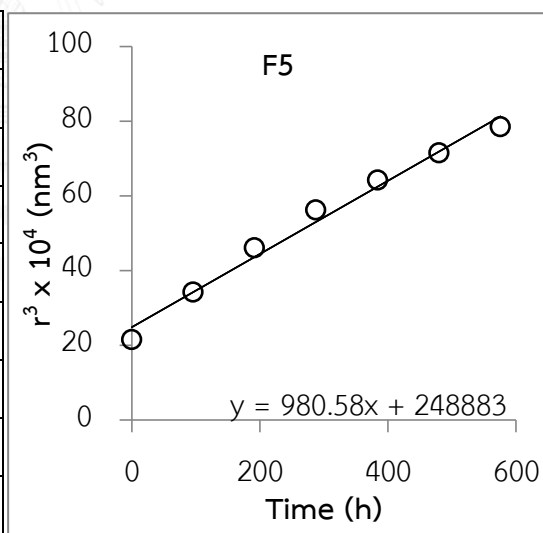
Heating-Cooling cycles

Cycle	At room temperature		At heating-cooling cycle	
	Size (d.nm)	PdI	Size (d.nm)	PdI
0	119.7 ± 1.4	0.173 ± 0.01	118.2 ± 1.39	0.173 ± 0.01
1	139.9 ± 0.91	0.106 ± 0.01	205.3 ± 1.72	0.071 ± 0.02
2	154.4 ± 1.06	0.095 ± 0.01	261.5 ± 2.59	0.121 ± 0.01
3	165.0 ± 1.82	0.086 ± 0.01	320.4 ± 1.82	0.097 ± 0.02
4	172.5 ± 1.12	0.083 ± 0.01	creaming	creaming
5	178.8 ± 1.27	0.083 ± 0.02	-	-
6	184.5 ± 1.27	0.070 ± 0.03	-	-

d.nm: diameter nanometer

Ostwald ripening rate at room temperature

Time (h)	Size (r.nm)	r^3 (nm ³)
0	59.9	214561.4
96	70.0	342507.8
192	77.2	459903.0
288	82.5	561291.0
384	86.3	641619.1
480	89.4	714648.9
576	92.2	784491.7
ω (nm ³ /h)	980.58	



r.nm: radius nanometer

 ω : Ostwald ripening rate

Table A-6 Physical stabilities of nanoemulsion F10

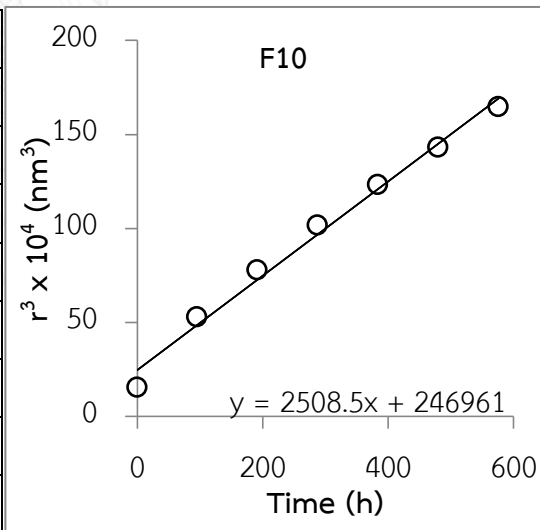
Heating-Cooling cycles

Cycle	At room temperature		At heating-cooling cycle	
	Size (d.nm)	Pdl	Size (d.nm)	Pdl
0	107.1 ± 0.15	0.118 ± 0.03	107.2 ± 0.15	0.118 ± 0.03
1	161.7 ± 1.39	0.061 ± 0.02	309.0 ± 2.63	0.137 ± 0.01
2	183.9 ± 1.39	0.058 ± 0.02	creaming	creaming
3	201.1 ± 1.84	0.072 ± 0.02	-	-
4	214.4 ± 1.88	0.078 ± 0.02	-	-
5	225.4 ± 0.95	0.077 ± 0.02	-	-
6	236.2 ± 2.63	0.117 ± 0.02	-	-

d.nm: diameter nanometer

Ostwald ripening rate at room temperature

Time (h)	Size (r.nm)	r^3 (nm ³)
0	53.5	153418.2
96	80.8	528278.3
192	92.0	777419.1
288	100.5	1016257.3
384	107.2	1231546.1
480	112.7	1431225.8
576	118.1	1647673.1
ω (nm ³ /h)	2508.5	



r.nm: radius nanometer

 ω : Ostwald ripening rate

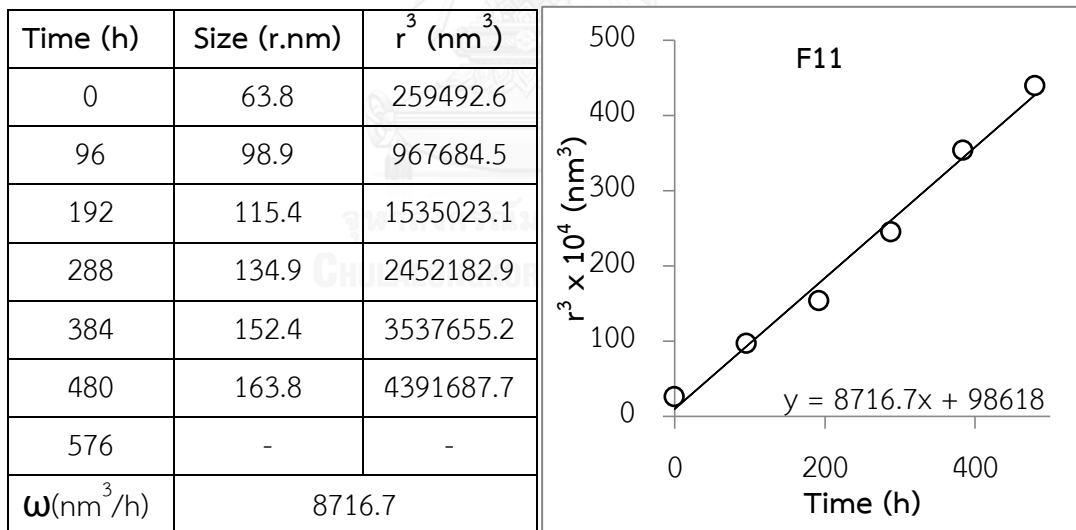
Table A-7 Physical stabilities of nanoemulsion F11

Heating-Cooling cycles

Cycle	At room temperature		At heating-cooling cycle	
	Size (d.nm)	Pdl	Size (d.nm)	Pdl
0	127.6 ± 0.38	0.074 ± 0.02	127.3 ± 0.38	0.074 ± 0.02
1	197.8 ± 2.30	0.074 ± 0.02	463.0 ± 5.28	0.096 ± 0.03
2	230.7 ± 2.22	0.070 ± 0.03	creaming	creaming
3	269.7 ± 1.68	0.114 ± 0.01	-	-
4	304.7 ± 3.78	0.107 ± 0.02	-	-
5	327.5 ± 2.21	0.117 ± 0.02	-	-
6	creaming	creaming	-	-

d.nm: diameter nanometer

Ostwald ripening rate at room temperature



r.nm: radius nanometer

 ω : Ostwald ripening rate

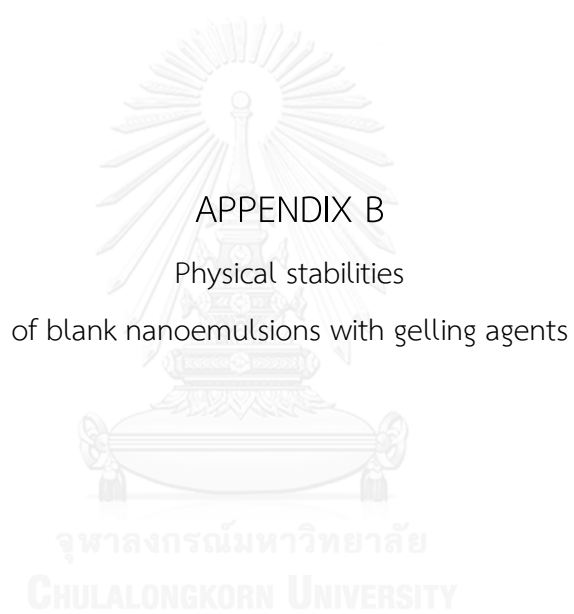


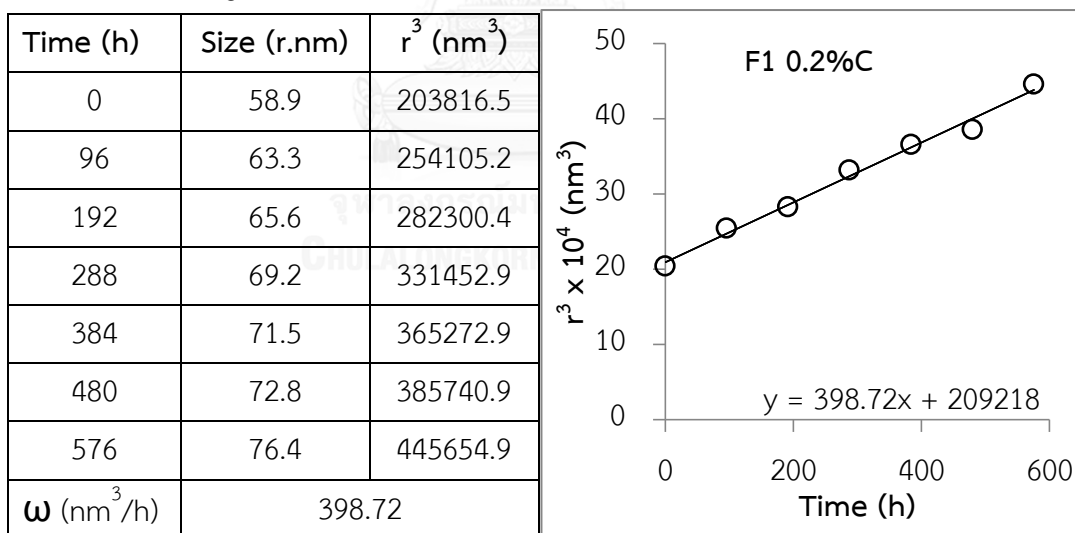
Table B-1 Physical stabilities of nanoemulsion F1 with 0.2 %w/w Carbopol® 940

Heating-Cooling cycles

Cycle	At room temperature		At heating-cooling cycle	
	Size (d.nm)	PdI	Size (d.nm)	PdI
0	117.7 ± 0.45	0.203 ± 0.01	117.4 ± 0.45	0.203 ± 0.11
1	126.7 ± 0.81	0.155 ± 0.01	163.6 ± 0.00	0.078 ± 0.00
2	131.2 ± 0.73	0.148 ± 0.01	184.9 ± 1.25	0.076 ± 0.01
3	138.4 ± 0.00	0.129 ± 0.00	210.0 ± 1.66	0.093 ± 0.02
4	143.0 ± 0.64	0.121 ± 0.02	227.3 ± 0.85	0.103 ± 0.01
5	145.6 ± 0.34	0.119 ± 0.01	245.8 ± 1.75	0.142 ± 0.01
6	152.8 ± 1.93	0.141 ± 0.01	277.2 ± 3.37	0.152 ± 0.03

d.nm: diameter nanometer

Ostwald ripening rate at room temperature



r.nm: radius nanometer

 ω : Ostwald ripening rate

Table B-2 Physical stabilities of nanoemulsion F4 with 0.15 %w/w Carbopol® 940

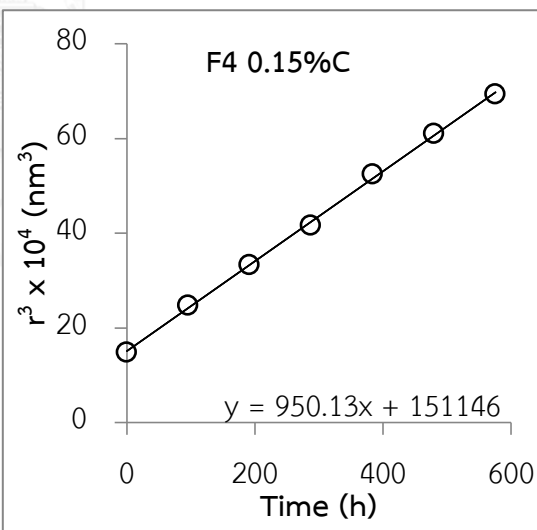
Heating-Cooling cycles

Cycle	At room temperature		At heating-cooling cycle	
	Size (d.nm)	PdI	Size (d.nm)	PdI
0	105.9 ± 0.89	0.172 ± 0.01	104.9 ± 0.89	0.172 ± 0.01
1	125.5 ± 0.57	0.114 ± 0.01	188.9 ± 2.10	0.070 ± 0.01
2	138.6 ± 1.34	0.105 ± 0.01	229.9 ± 0.42	0.060 ± 0.01
3	149.4 ± 2.00	0.097 ± 0.01	261.3 ± 1.76	0.106 ± 0.00
4	161.2 ± 0.90	0.071 ± 0.01	creaming	creaming
5	169.7 ± 0.66	0.054 ± 0.03	-	-
6	177.1 ± 1.84	0.075 ± 0.02	-	-

d.nm: diameter nanometer

Ostwald ripening rate at room temperature

Time (h)	Size (r.nm)	r^3 (nm ³)
0	53.0	148456.0
96	62.8	247277.0
192	69.3	332935.0
288	74.7	416414.4
384	80.6	523928.3
480	84.8	610523.2
576	88.5	693941.6
ω (nm ³ /h)	950.13	



r.nm: radius nanometer

 ω : Ostwald ripening rate

Table B-3 Physical stabilities of nanoemulsion F4 with 0.175 %w/w Carbopol[®]
940

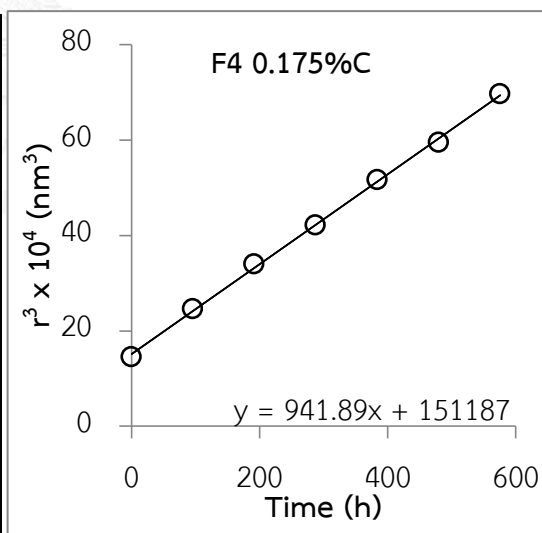
Heating-Cooling cycles

Cycle	At room temperature		At heating-cooling cycle	
	Size (d.nm)	Pdl	Size (d.nm)	Pdl
0	105.0 ± 1.16	0.186 ± 0.02	103.9 ± 1.16	0.186 ± 0.02
1	125.2 ± 0.17	0.131 ± 0.01	193.1 ± 1.53	0.063 ± 0.02
2	139.5 ± 1.01	0.102 ± 0.03	238.2 ± 1.84	0.117 ± 0.01
3	149.9 ± 2.29	0.095 ± 0.01	289.5 ± 1.12	0.163 ± 0.00
4	160.4 ± 2.17	0.084 ± 0.00	creaming	creaming
5	168.2 ± 2.31	0.075 ± 0.01	-	-
6	177.3 ± 1.37	0.084 ± 0.01	-	-

d.nm: diameter nanometer

Ostwald ripening rate at room temperature

Time (h)	Size (r.nm)	r^3 (nm ³)
0	52.5	144566.7
96	62.6	245414.3
192	69.7	33924.1
288	74.9	420610.6
384	80.2	515849.6
480	84.1	594823.3
576	88.7	696684.6
ω (nm ³ /h)	941.89	



r.nm: radius nanometer

ω : Ostwald ripening rate

Table B-4 Physical stabilities of nanoemulsion F4 with 0.2 %w/w Carbopol® 940

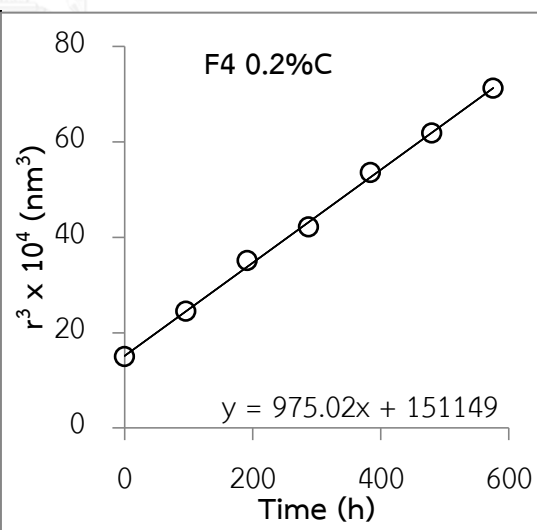
Heating-Cooling cycles

Cycle	At room temperature		At heating-cooling cycle	
	Size (d.nm)	PDI	Size (d.nm)	PDI
0	105.7 ± 1.11	0.179 ± 0.00	104.5 ± 1.11	0.179 ± 0.00
1	124.9 ± 1.18	0.124 ± 0.01	195.9 ± 1.67	0.065 ± 0.03
2	141.0 ± 1.30	0.101 ± 0.01	245.5 ± 1.30	0.113 ± 0.00
3	149.8 ± 2.73	0.090 ± 0.02	290.1 ± 4.85	0.121 ± 0.00
4	162.3 ± 1.63	0.081 ± 0.01	342.5 ± 0.00	0.162 ± 0.00
5	170.3 ± 1.13	0.076 ± 0.00	creaming	creaming
6	178.5 ± 1.44	0.080 ± 0.02	-	-

d.nm: diameter nanometer

Ostwald ripening rate at room temperature

Time (h)	Size (r.nm)	r^3 (nm ³)
0	52.9	147616.5
96	62.5	243555.2
192	70.5	350030.0
288	74.9	420467.5
384	81.1	533905.2
480	85.2	6174382.0
576	89.2	710723.4
ω (nm ³ /h)	975.02	



r.nm: radius nanometer

 ω : Ostwald ripening rate

Table B-5 Physical stabilities of nanoemulsion F4 with 0.1 %w/w HPMC E5

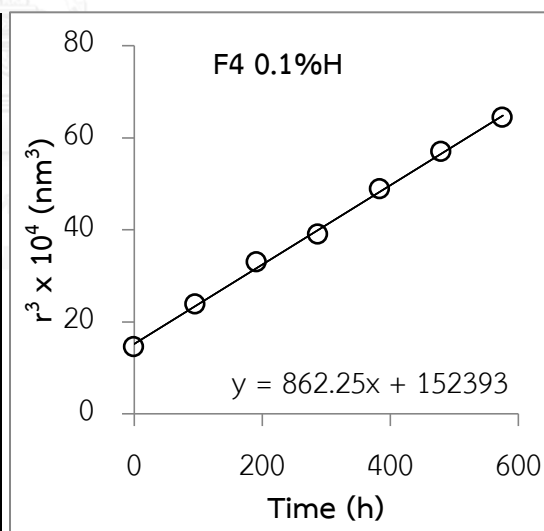
Heating-Cooling cycles

Cycle	At room temperature		At heating-cooling cycle	
	Size (d.nm)	PdI	Size (d.nm)	PdI
0	105.2 ± 1.02	0.175 ± 0.01	104.0 ± 1.02	0.175 ± 0.01
1	124.0 ± 0.78	0.115 ± 0.02	187.2 ± 1.30	0.037 ± 0.01
2	138.1 ± 1.13	0.098 ± 0.01	210.2 ± 0.42	0.045 ± 0.01
3	146.2 ± 1.46	0.066 ± 0.01	creaming	creaming
4	157.5 ± 1.74	0.090 ± 0.00	-	-
5	165.8 ± 0.78	0.066 ± 0.01	-	-
6	172.7 ± 1.04	0.070 ± 0.03	-	-

d.nm: diameter nanometer

Ostwald ripening rate at room temperature

Time (h)	Size (r.nm)	r^3 (nm ³)
0	52.6	145394.7
96	62.0	238039.8
192	69.1	329459.7
288	73.1	390353.4
384	78.8	488373.0
480	82.9	569207.5
576	86.4	644222.6
ω (nm ³ /h)	862.25	



r.nm: radius nanometer

 ω : Ostwald ripening rate

Table B-6 Physical stabilities of nanoemulsion F5 with 0.15 %w/w Carbopol® 940

Heating-Cooling cycles

Cycle	At room temperature		At heating-cooling cycle	
	Size (d.nm)	PdI	Size (d.nm)	PdI
0	101.0 ± 0.46	0.187 ± 0.02	100.5 ± 0.46	0.187 ± 0.02
1	124.2 ± 0.78	0.118 ± 0.02	189.5 ± 0.83	0.056 ± 0.01
2	140.6 ± 1.20	0.104 ± 0.02	223.5 ± 2.31	0.064 ± 0.03
3	150.2 ± 1.96	0.092 ± 0.02	259.4 ± 1.70	0.102 ± 0.00
4	161.6 ± 1.67	0.080 ± 0.01	creaming	creaming
5	170.7 ± 2.38	0.090 ± 0.02	-	-
6	178.9 ± 2.00	0.088 ± 0.02	-	-

d.nm: diameter nanometer

Ostwald ripening rate at room temperature

Time (h)	Size (r.nm)	r^3 (nm ³)
0	50.5	128787.6
96	62.1	239581.4
192	70.3	347555.0
288	75.1	423141.9
384	80.8	527024.6
480	85.3	621556.8
576	89.4	71470.8
ω (nm ³ /h)	1004.9	

r.nm: radius nanometer

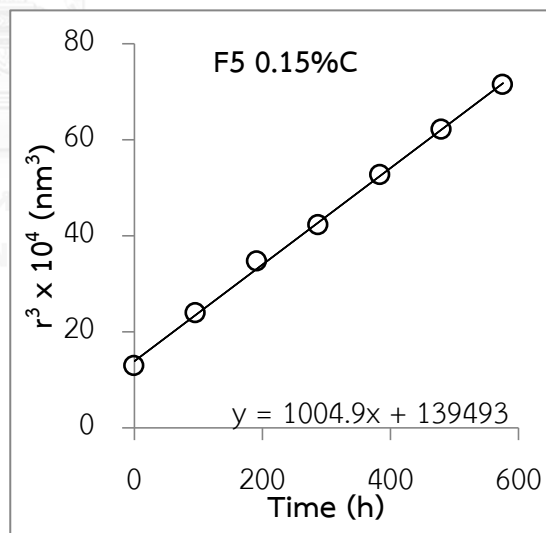
 ω : Ostwald ripening rate

Table B-7 Physical stabilities of nanoemulsion F5 with 0.175 %w/w Carbopol[®]
940

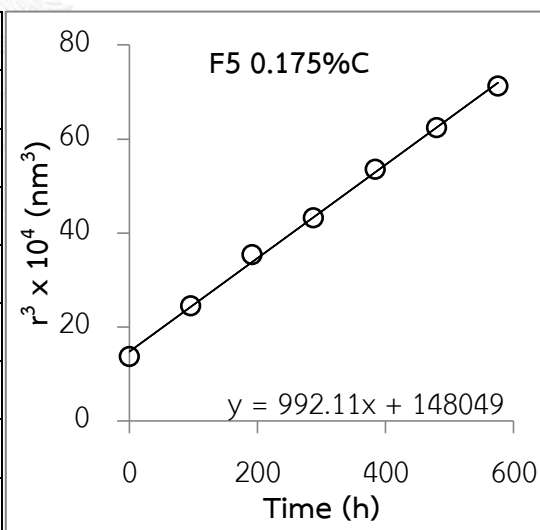
Heating-Cooling cycles

Cycle	At room temperature		At heating-cooling cycle	
	Size (d.nm)	Pdl	Size (d.nm)	Pdl
0	103.0 ± 0.46	0.174 ± 0.03	102.5 ± 0.46	0.174 ± 0.03
1	125.0 ± 0.83	0.115 ± 0.02	192.0 ± 0.94	0.069 ± 0.02
2	141.4 ± 0.40	0.111 ± 0.01	234.0 ± 1.63	0.097 ± 0.001
3	151.2 ± 2.07	0.100 ± 0.00	281.0 ± 1.61	0.131 ± 0.00
4	162.4 ± 1.32	0.080 ± 0.01	creaming	creaming
5	170.9 ± 2.33	0.077 ± 0.02	-	-
6	178.6 ± 0.47	0.066 ± 0.03	-	-

d.nm: diameter nanometer

Ostwald ripening rate at room temperature

Time (h)	Size (r.nm)	r^3 (nm ³)
0	51.5	136722.2
96	62.5	244041.0
192	70.7	353018.5
288	75.6	431798.4
384	81.2	535387.3
480	85.4	623744.3
576	89.3	711727.3
ω (nm ³ /h)	992.11	



r.nm: radius nanometer

ω : Ostwald ripening rate

Table B-8 Physical stabilities of nanoemulsion F5 with 0.2 %w/w Carbopol® 940

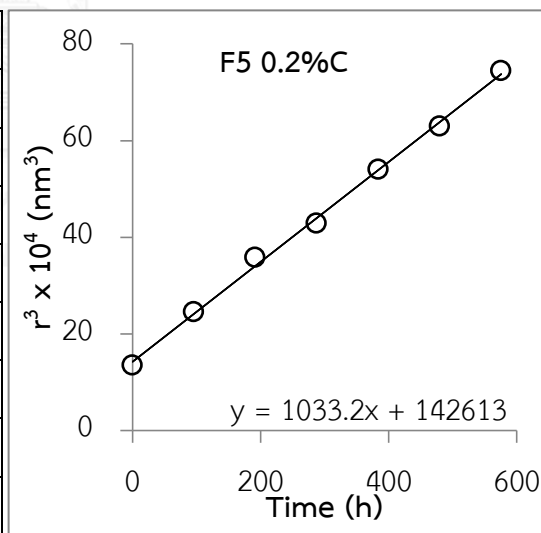
Heating-Cooling cycles

Cycle	At room temperature		At heating-cooling cycle	
	Size (d.nm)	PdI	Size (d.nm)	PdI
0	102.7 ± 1.10	0.186 ± 0.01	101.4 ± 1.10	0.186 ± 0.01
1	125.2 ± 0.87	0.126 ± 0.02	195.0 ± 1.53	0.068 ± 0.01
2	142.0 ± 1.20	0.111 ± 0.01	244.9 ± 0.97	0.122 ± 0.01
3	150.8 ± 1.04	0.102 ± 0.01	292.0 ± 0.96	0.146 ± 0.00
4	162.9 ± 1.27	0.090 ± 0.01	358.8 ± 0.00	0.125 ± 0.00
5	171.4 ± 1.63	0.089 ± 0.01	creaming	creaming
6	181.2 ± 1.18	0.073 ± 0.02	-	-

d.nm: diameter nanometer

Ostwald ripening rate at room temperature

Time (h)	Size (r.nm)	r^3 (nm ³)
0	51.3	135270.4
96	62.6	245414.3
192	71.0	358039.6
288	75.4	428379.7
384	81.5	540347.6
480	85.7	629610.1
576	90.6	744083.8
ω (nm ³ /h)	1033.2	



r.nm: radius nanometer

 ω : Ostwald ripening rate

Table B-9 Physical stabilities of nanoemulsion F5 with 0.1 %w/w HPMC E5

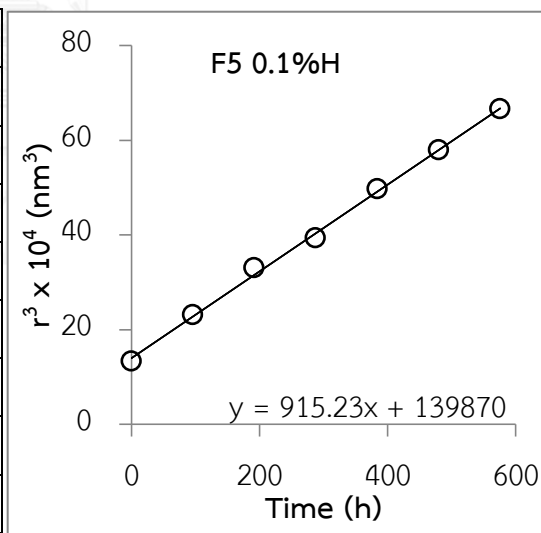
Heating-Cooling cycles

Cycle	At room temperature		At heating-cooling cycle	
	Size (d.nm)	PdI	Size (d.nm)	PdI
0	101.9 ± 0.90	0.166 ± 0.01	101.0 ± 0.90	0.166 ± 0.01
1	122.7 ± 0.47	0.117 ± 0.02	186.8 ± 1.46	0.051 ± 0.01
2	138.1 ± 1.58	0.083 ± 0.02	215.9 ± 1.60	0.035 ± 0.02
3	146.4 ± 1.16	0.085 ± 0.02	creaming	creaming
4	158.3 ± 1.51	0.062 ± 0.01	-	-
5	166.7 ± 2.76	0.058 ± 0.02	-	-
6	174.6 ± 2.07	0.063 ± 0.02	-	-

d.nm: diameter nanometer

Ostwald ripening rate at room temperature

Time (h)	Size (r.nm)	r^3 (nm ³)
0	51.0	132389.8
96	61.3	230724.3
192	69.1	329345.3
288	73.2	392086.5
384	79.2	496163.0
480	83.3	578530.1
576	87.3	664961.4
ω (nm ³ /h)	915.23	



r.nm: radius nanometer

 ω : Ostwald ripening rate

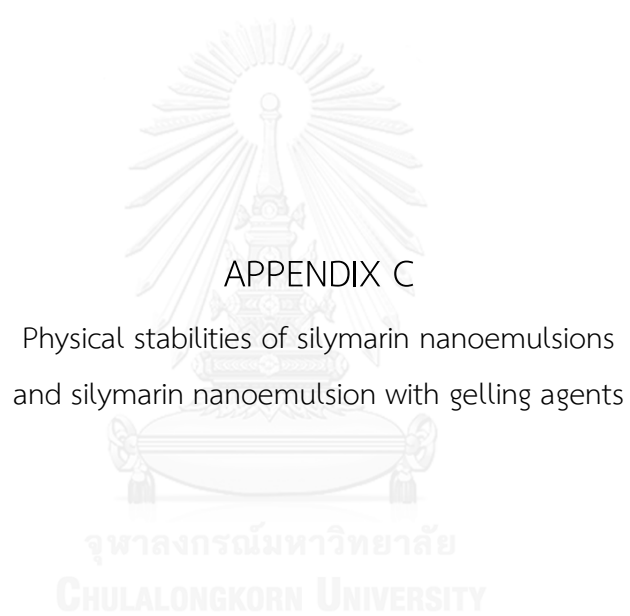


Table C-1 Physical stabilities of 0.5 %w/w silymarin nanoemulsion F1

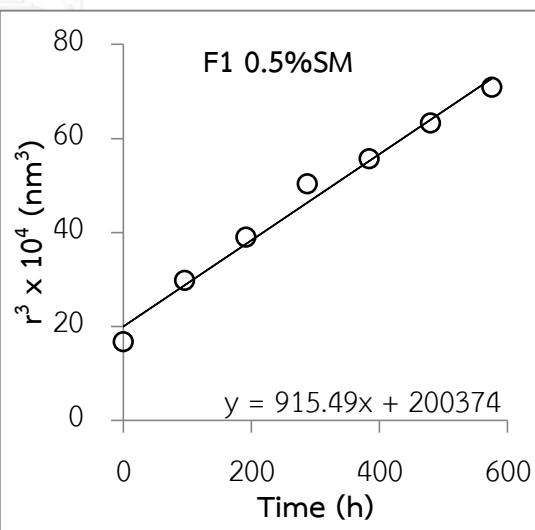
Heating-Cooling cycles

Cycle	At room temperature		At heating-cooling cycle	
	Size (d.nm)	PdI	Size (d.nm)	PdI
0	109.9 ± 0.45	0.177 ± 0.01	109.9 ± 0.45	0.177 ± 0.01
1	133.4 ± 1.26	0.113 ± 0.02	311.10 ± 2.52	0.111 ± 0.00
2	145.9 ± 0.65	0.103 ± 0.02	444.41 ± 4.74	0.101 ± 0.04
3	159.0 ± 0.00	0.088 ± 0.00	creaming	creaming
4	164.4 ± 1.04	0.068 ± 0.02	-	-
5	171.6 ± 1.62	0.077 ± 0.01	-	-
6	178.2 ± 1.40	0.080 ± 0.02	-	-

d.nm: diameter nanometer

Ostwald ripening rate at room temperature

Time (h)	Size (r.nm)	r^3 (nm ³)
0	55.0	166071.2
96	66.7	296814.4
192	73.0	388481.7
288	79.5	502459.9
384	82.2	555412.2
480	85.8	631264.4
576	89.1	707741.0
ω (nm ³ /h)	915.49	



r.nm: radius nanometer

 ω : Ostwald ripening rate

Table C-2 Physical stabilities of 0.75 %w/w silymarin nanoemulsion F1

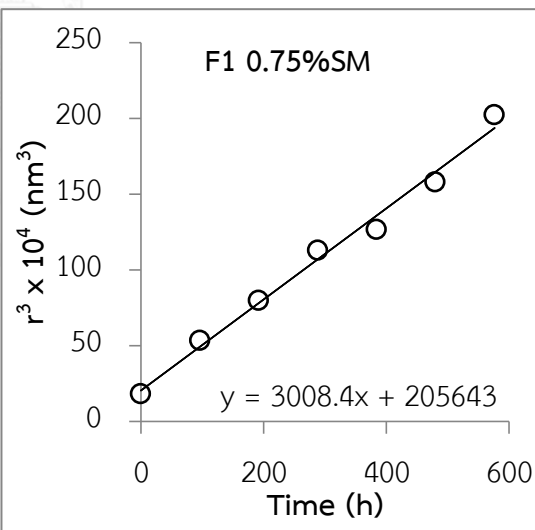
Heating-Cooling cycles

Cycle	At room temperature		At heating-cooling cycle	
	Size (d.nm)	PdI	Size (d.nm)	PdI
0	113.0 ± 1.20	0.159 ± 0.01	113.0 ± 1.20	0.159 ± 0.01
1	162.2 ± 0.89	0.073 ± 0.02	creaming	creaming
2	185.4 ± 0.97	0.068 ± 0.02	-	-
3	208.2 ± 0.00	0.094 ± 0.00	-	-
4	216.3 ± 0.00	0.084 ± 0.00	-	-
5	232.8 ± 1.33	0.106 ± 0.01	-	-
6	253.0 ± 1.63	0.114 ± 0.01	-	-

d.nm: diameter nanometer

Ostwald ripening rate at room temperature

Time (h)	Size (r.nm)	r^3 (nm ³)
0	56.5	180362.1
96	81.1	533845.9
192	92.7	796172.7
288	104.1	1128111.9
384	108.1	1264389.2
480	116.4	1577546.1
576	126.5	2024020.6
ω (nm ³ /h)	3008.4	



r.nm: radius nanometer

 ω : Ostwald ripening rate

Table C-3 Physical stabilities of 1 %w/w silymarin nanoemulsion F1

Heating-Cooling cycles

Cycle	At room temperature		At heating-cooling cycle	
	Size (d.nm)	PdI	Size (d.nm)	PdI
0	136.9 ± 0.30	0.097 ± 0.01	136.6 ± 0.30	0.097 ± 0.01
1	254.7 ± 2.58	0.132 ± 0.02	creaming	creaming
2	360.0 ± 2.56	0.184 ± 0.02	-	-
3	426.4 ± 0.00	0.127 ± 0.00	-	-
4	450.6 ± 1.76	0.096 ± 0.00	-	-
5	527.9 ± 5.44	0.199 ± 0.01	-	-
6	581.3 ± 2.81	0.214 ± 0.01	-	-

d.nm: diameter nanometer

Ostwald ripening rate at room temperature

Time (h)	Size (r.nm)	r^3 (nm ³)
0	68.5	320715.8
96	127.4	2065632.8
192	180.0	5832534.6
288	213.2	9693094.1
384	225.3	11433735.8
480	264.0	18389291.6
576	290.7	24553362.8
ω (nm ³ /h)	41275	

r.nm: radius nanometer

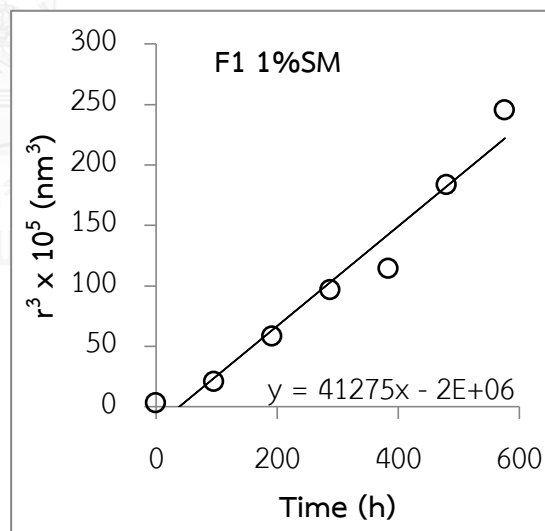
 ω : Ostwald ripening rate

Table C-4 Physical stabilities of 0.5 %w/w silymarin nanoemulsion F5

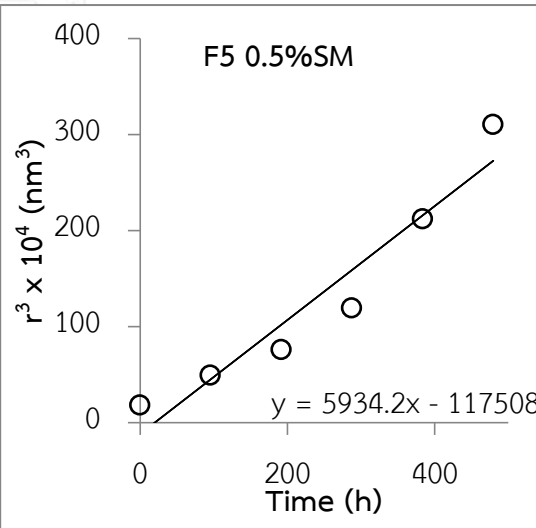
Heating-Cooling cycles

Cycle	At room temperature		At heating-cooling cycle	
	Size (d.nm)	PdI	Size (d.nm)	PdI
0	112.5 ± 0.56	0.141 ± 0.03	112.6 ± 0.56	0.141 ± 0.028
1	157.8 ± 1.71	0.074 ± 0.03	599.7 ± 16.24	0.428 ± 0.031
2	182.5 ± 1.69	0.051 ± 0.02	creaming	creaming
3	211.9 ± 2.14	0.087 ± 0.04	-	-
4	256.8 ± 2.54	0.137 ± 0.02	-	-
5	291.8 ± 4.38	0.199 ± 0.01	-	-
6	creaming	creaming	-	-

d.nm: diameter nanometer

Ostwald ripening rate at room temperature

Time (h)	Size (r.nm)	r^3 (nm ³)
0	56.3	178135.2
96	78.9	491477.3
192	91.3	759798.8
288	106.0	1189331.4
384	128.4	2116453.9
480	145.9	3105043.2
576	-	-
ω (nm ³ /h)	5934.2	



The figure is a scatter plot titled "F5 0.5%SM". The vertical axis (y-axis) is labeled $r^3 \times 10^4$ (nm³) and ranges from 0 to 400. The horizontal axis (x-axis) is labeled "Time (h)" and ranges from 0 to 400. There are seven data points plotted as open circles. A solid black line represents a linear regression fit to the data. The equation for the line is $y = 5934.2x - 117508$.

r.nm: radius nanometer

 ω : Ostwald ripening rate

Table C-5 Physical stabilities of 0.75 %w/w silymarin nanoemulsion F5

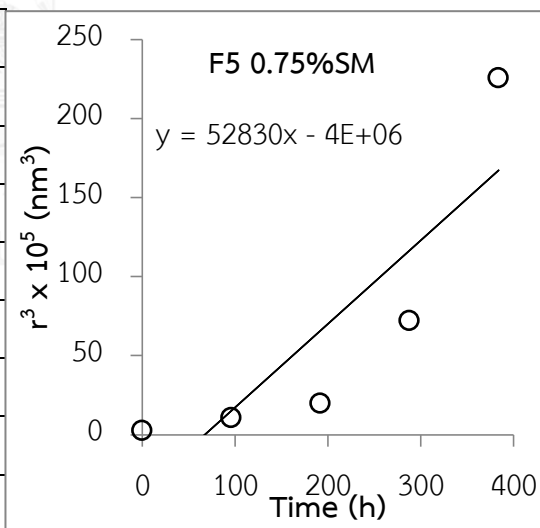
Heating-Cooling cycles

Cycle	At room temperature		At heating-cooling cycle	
	Size (d.nm)	PdI	Size (d.nm)	PdI
0	119.8 ± 1.90	0.118 ± 0.00	118.9 ± 1.90	0.118 ± 0.00
1	202.9 ± 1.54	0.074 ± 0.03	creaming	creaming
2	248.9 ± 1.87	0.114 ± 0.02	-	-
3	385.4 ± 2.95	0.263 ± 0.02	-	-
4	564.8 ± 8.63	0.416 ± 0.02	-	-
5	creaming	creaming	-	-
6	-	-	-	-

d.nm: diameter nanometer

Ostwald ripening rate at room temperature

Time (h)	Size (r.nm)	r^3 (nm ³)
0	59.9	2147685.1
96	101.5	1044133.8
192	124.4	1926690.5
288	192.7	7155585.0
384	282.4	22517384.8
480	-	-
576	-	-
ω (nm ³ /h)	52830	



r.nm: radius nanometer

 ω : Ostwald ripening rate

Table C-6 Physical stabilities of 0.5 %w/w silymarin nanoemulsion F1 with 0.2 %w/w Carbopol[®] 940

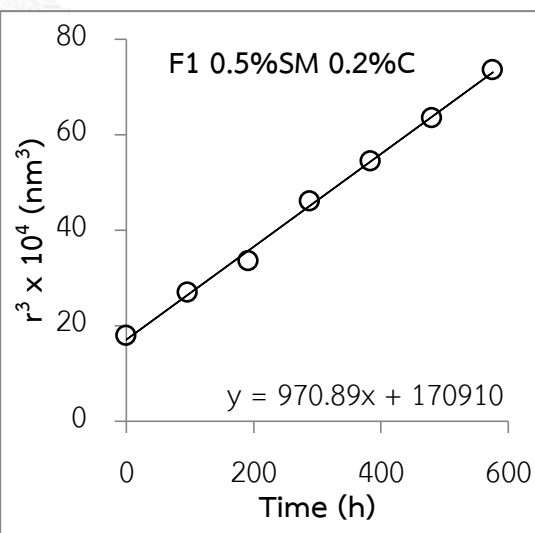
Heating-Cooling cycles

Cycle	At room temperature		At heating-cooling cycle	
	Size (d.nm)	Pdl	Size (d.nm)	Pdl
0	112.7 ± 0.51	0.208 ± 0.00	112.5 ± 0.51	0.208 ± 0.12
1	129.0 ± 0.52	0.142 ± 0.02	330.8 ± 0.00	0.150 ± 0.00
2	138.8 ± 1.27	0.125 ± 0.01	470.2 ± 5.90	0.152 ± 0.02
3	154.4 ± 0.00	0.102 ± 0.00	664.0 ± 7.46	0.252 ± 0.02
4	163.3 ± 1.13	0.091 ± 0.02	699.8 ± 10.27	0.216 ± 0.03
5	171.8 ± 1.16	0.091 ± 0.02	786.9 ± 6.21	0.204 ± 0.01
6	180.5 ± 1.65	0.086 ± 0.01	882.1 ± 18.36	0.242 ± 0.04

d.nm: diameter nanometer

Ostwald ripening rate at room temperature

Time (h)	Size (r.nm)	r^3 (nm ³)
0	56.3	178772.3
96	64.5	268267.5
192	69.4	334175.9
288	77.2	459706.4
384	81.6	543838.0
480	85.9	633839.8
576	90.3	735091.9
ω (nm ³ /h)	970.89	



r.nm: radius nanometer

ω : Ostwald ripening rate

Table C-7 Physical stabilities of 0.75 %w/w silymarin nanoemulsion F1 with 0.2 %w/w Carbopol[®] 940

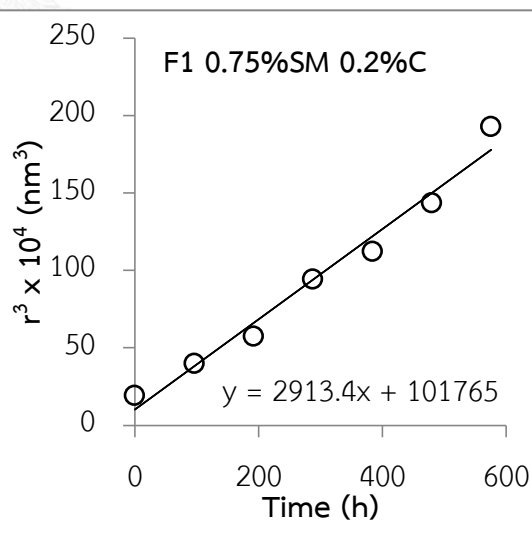
Heating-Cooling cycles

Cycle	At room temperature		At heating-cooling cycle	
	Size (d.nm)	Pdl	Size (d.nm)	Pdl
0	115.0 ± 0.912	0.185 ± 0.03	116.4 ± 0.92	0.185 ± 0.10
1	147.2 ± 1.01	0.099 ± 0.02	640.6 ± 0.00	0.158 ± 0.00
2	166.0 ± 1.49	0.091 ± 0.02	1128.1 ± 18.17	0.285 ± 0.02
3	196.1 ± 0.00	0.077 ± 0.00	1287.0 ± 22.06	0.285 ± 0.02
4	207.8 ± 1.61	0.097 ± 0.02	1549.9 ± 26.93	0.224 ± 0.02
5	225.6 ± 2.71	0.099 ± 0.01	1670.1 ± 33.53	0.215 ± 0.05
6	248.8 ± 0.62	0.131 ± 0.03	creaming	creaming

d.nm: diameter nanometer

Ostwald ripening rate at room temperature

Time (h)	Size (r.nm)	r^3 (nm ³)
0	57.5	190109.4
96	73.6	398330.8
192	83.0	572014.4
288	98.1	942633.3
384	103.9	1121347.1
480	112.8	1435249.2
576	124.4	1926156.3
ω (nm ³ /h)	2913.4	



r.nm: radius nanometer

ω : Ostwald ripening rate

VITA

Miss Ranit Charoenjittichai was born on November 2, 1988 in Chiangrai province, Thailand. She graduated with the Bachelor's degree of Science in Cosmetic Science from Mae Fah Luang University in 2009. She entered the Master's degree of Science in Pharmaceutical Technology at Chulalongkorn University in 2013.

